ELECTRICAL TRANSPORT AND THE SCHOTTKY EFFECT IN ORGANIC NANOELECTRONIC MATERIALS AND DEVICES

BY

WUDYALEW WONDMAGEGN, B.Sc., M.Sc.

A dissertation submitted to the Graduate School

in partial fulfillment of the requirements

for the degree

Doctor of Philosophy

Electrical Engineering

New Mexico State University

Las Cruces, New Mexico

December 2007

"Electrical Transport and the Schottky Effect in Organic Nanoelectronic Materials and Devices," a thesis prepared by Wudyalew Wondmagegn in partial fulfillment of the requirements for the degree, Doctor of Philosophy, has been approved and accepted by the following:

_____

Linda Lacey
Dean of the Graduate School

_____

Dr. Paul M. Furth
Chair of the Examining Committee

_____

Date

Committee in charge:

Dr. David Voelz

Dr. Igor Vasiliev

Dr. Robert Armstrong

ACKNOWLEDGMENT

During this work I have collaborated with many people for whom I have great regard, and I wish to extend my warmest thanks to all those who have helped me with my work. First, I would like to forward my deepest gratitude to my advisor, Dr. Paul Furth, for his unlimited and brotherly advice, suggestions and comments. I would like to gratefully acknowledge Dr. Seamus Curran for letting me work on this project in his lab. I am also thankful to my colleagues and collaborators - James Dewald, Dr. Michael DeAntonio, Dr. Amanda Ellis, Dr. Donghui Zhang, Jamal Thalla, Sampath Dias, Yvonne Tores, Aditya Avadhanula, and others in the nanophysics group - for their participation in valuable experiments and discussions.

I would like to express my sincere thanks to Dr. David Voelz for his financial support for the last couple of years of my study and for being on my committee. I am also thankful to Dr. Igor Vasiliev for his time and effort in reviewing and commenting on my dissertation proposal. I am very grateful to Dr Robert Armstrong for being on my dissertation committee.

I would also like to thank the Physics and EE departments and my instructors for their help in one way or another for my success. Many thanks go in particular to Dr. Charles Bruce and Dr. Robert Liefeld for teaching me how to work on an ultra high vacuum system.

Finally, I would like to express my deepest appreciation and love to my wife Alemitu Minalu and my sons Nathnael and Bereketab for their love and patience with me during this period. They have lost a lot due to this research I was involved in

during the years of my study. Without their encouragement and understanding, it would have been impossible for me to finish this work.

Don't be impatient for the Lord to act!

Travel steadily along his path.

He will honor you, giving you the land.

You will see the wicked destroyed.

(Psalm 37:34)

Amen

ABSTRACT

The field of nanotechnology is emerging with the promise of cheap, light weight, and flexible optoelectronics devices. Some commercial applications based on semiconducting polymers have already become available in the market. This field has also brought new challenges for the research community.

In this work, the electrical transport and spectroscopic properties of different nanomaterials and nanocomposites have been studied. The composites were made from polymers, nanotubes, metallic nanoparticles, and dyes. Electrical transport and Schottky effect are the properties that fundamentally govern the operation of the three dominant types of organic electronic devices such as organic light emitting devices (OLEDs), photosensitive devices (solar cells and photodetectors), and organic field effect transistors (OFETs).

Schottky devices have been made from pristine nanomaterials and nanocomposites. The Thermionic emission/diffusion equation has been used to extract the parameters of the device. Their performance has been studied and compared. Devices made from composites have shown better performance than those that are made of pristine polymers. Enhancement of light absorption has also been observed by attaching dyes to single wall nanotubes.

TABLE OF CONTENTS

TABLE OF FIGURES

LIST OF SYMBOLS

μ - mobility

Δ - Coulomb barrier energy

γ - mean inverse hopping distance

k_B – Boltzmann's constant

σ – conductivity

χ_s – electron affinity

ϕ_s - work function of semiconductor

E_c - conduction band energy

E_F - Fermi energy level

ϕ_{bn} - barrier encountered by electrons in the metal

V_{bi} - built-in potential encountered by electrons in the semiconductor

E_g - bandgap of the semiconductor

ϕ_0 - position of neutral level measured from the top of the valence band

ε_i - permittivity of oxide layer

δ – thickness of oxide layer

D_s - density of surface states

J - current density

Js - saturation current density

q - absolute electron charge

m^*- effective electron mass

h - Planck's constant

T - absolute temperature

n - ideality factor

I_{gr} - generation-recombination current

I_{gr0} - saturation generation-recombination component

n_i - intrinsic carrier concentration

τ - effective carrier lifetime in the depletion region

I_{Tn0} - tunneling saturation current

E_0 - tunneling constant

E_{00} - a tunneling parameter inherently related to material properties of the semiconductor

R_{lk} - leakage resistor

I_{lk} - leakage current

Al - Aluminium

Au – Gold

C_{60} - Fullerene

σ_c - conductivity of the composite.

σ_n - conductivity of the nanotube

σ_p - conductivity of the pristine polymer

p - mass fraction of the nanotube

b - empirical parameter

p_c - percolation threshold (or ballistic threshold)

LIST OF ABBREVIATIONS

OLED – Organic Light Emitting Diode

OFET – Organic Field Effect Transistors

PmPV - poly(*m*-phenylenevinylene-co-2,5-dioctoxy-p-phenylenevinylene

SWNT – Single Wall NanoTube

DOS – Density Of States

PPV – Poly Phenylene Vinylene

SSH - Su-Schrieffer-Heeger model

MDP – Molecularly Doped Polymer

GDM – Gaussian Disorder Model

MS – Metal Semiconductor

PV - Photovoltaic

UV-Vis – Ultraviolet Visible

NSOM – Near field Scanning Optical Microscope

ITO – Indium Thin Oxide

MEMS - Micro Electro Mechanical Systems

NEMS - Nano Electro Mechanical Systems

MWCNT - Multi-Walled Carbon Nanotubes

THF – Tetrahydrofuran (1,4-epoxy-butane)

1. INTRODUCTION

The history of research on plastic electronics began in the 1970's and 1980's when researchers found that the conductivity of certain polymeric systems could be changed over the full range from insulator to metal by chemical doping. The first polymer capable of conducting electricity - polyacetylene – was prepared by Shirakawa [217]. The subsequent discovery by Heeger and MacDiarmid [100] that the polymer would undergo an increase in conductivity of 10 orders of magnitude by oxidative doping helped raise the world's interest in such materials. Since then this field has seen much progress, to the extent that researchers are able to enhance physical properties at the nano-scale level. These developments led to the emergence of nanotechnology in all areas of science and engineering.

1.1 Motivation

The birth of material engineering in the nanometer scale has generated new materials and systems with enhanced physical properties that could potentially revolutionize the electronic and photonic industry by combining the advantages of low cost of fabrication, strength, and flexibility.

The potential advantage anticipated in materials engineering has motivated many researchers to work in this field. More researchers continue to join the field and more publications are being generated each year. Nowadays, nanotechnology is a very active research subject spanning many areas, including materials development, device design, deposition processes, and modeling. Some commercial applications

based on semiconducting polymers, also known as organic semiconductors, have already become available on the market, such as a Pioneer car radio with Organic Light-Emitting Diodes (OLED) display, Motorola's timeport color OLED cell phone, and Kodak's color OLED digital camera. In addition, a Philips shaver and a Philips mobile phone both feature an OLED display [246].

Although all of these devices are OLED with traditional Si-based backplanes and control electronics, they are a tremendous step toward realizing an organic share of the electronics markets. In addition to OLEDs, there is also an effort to make other devices using organic semiconductors. There is a good progress made in the realization of organic transistors [199][216], organic sensors [[226][270], organic memories [163][212], and possibly smart textiles [135][246]. Optically pumped organic lasers have also been demonstrated at UV, visible, and IR wavelengths [30][126]. Photodetectors with collection efficiencies as high as 80% [184][186], and solar cells with power conversion efficiencies as high as 5.2% have been reported [196]. Organic thin-film transistors with excellent electrical characteristics and low operating voltages (below 2 V) have been reported [113]. If certain problems are surmounted, integrated circuits fabricated from organic thin-film transistors will have the potential of enabling cheap and well-performing logic circuits. Applications of these thin-film transistors are as diverse as electronic price tags, postage stamps, radio-frequency identification tags, and smart cards [67][234].

Despite such a significant development seen over the past decades, there is still a lot to be done to improve the quality of such devices in terms of electronic

properties, optical properties, stability, and processability, or manufacturability. We still await the key applications that may drive organic electronics toward a mature industrial discipline. Significant improvement is needed in order to provide comparable device performance and cost with the already existing inorganic devices, in particular, silicon. Different strategies are underway, such as enhancing properties by forming composites from different materials, using hybrid organic/inorganic systems [10][162], and designing systems that combine the performance of silicon based electronics with the functionality of organic components [97][161][192]. The desirable functions provided by organic components are sensing, flexibility, and actuation.

1.2 Aims, objectives, and layout of the dissertation

The objective of this research is to test the electrical transport property of different nanocomposites and to make Schottky diodes and solar cells from them. The composites are made from polymers, nanotubes, metallic nanoparticles, and dyes. With this goal in mind, a wide variety of composites will be tested for conductivity and Schottky effect.

Electrical transport and Schottky effect are the properties that fundamentally govern the operation of the three dominant types of organic electronic devices, such as organic light emitting devices (OLEDs), photosensitive devices (solar cells and photodetectors), and organic field effect transistors (OFETs).

In chapter two of this dissertation we present the theoretical background for

electrical transport in organic semiconductors and Schottky effect at metal semiconductor junctions. In chapter three, we present a literature review of the developments in organic solar cells and other organic electronic devices. In chapters four, five, and six we present all of our experimental results from a variety of organic composites. Finally we will summarize the thesis and point out possible future extensions of this work in chapter 7.

1.3 Contributions

The original contributions of this dissertation are listed below:

- Schottcky diodes based on PmPV- Gold nanocomposite
- Electrical and spectroscopic characteristics of PmPV- C_{60} composite
- Electrical transport property of Polystyrene-Nanotube composite with two profile percolation effect.
- Schottky diodes based on Dye-Nanotube-Polymer composite

A list of papers and a patent application based on this dissertation is given below

1. W.T. Wondmagegn and S.A. Curran, "A study of C60–poly(m-phenylenevinylene-co-2,5-dioctoxy-p-3 phenylenevinylene) nanocomposite," *Thin Solid Films* 515 (2006) 2393–2397

2. S. A. Curran, Donghui Zhang, W. T. Wondmagegn, Amanda V. Ellis, Jiri Cech, Siegmar Roth, and David L. Carroll, "Dynamic electrical properties of polymer-carbon nanotube composites: Enhancement through covalent bonding," *J. Mater. Res*., Vol. 21, No. 4, Apr 2006

3. J. L. Dewald, W. T. Wondmagegn, Amanda V. Ellis and Seamus A. Curran,

"Enhanced rectification through polymer-gold nanoparticle interaction**,"** *Synthetic Metals* 155 (2005) 39–44

4. J. L. Dewald, A. V. Ellis, W. Wondmagegn and S. A. Curran, "Composite formation and Electronic Properties of gold-polymeric nanocomposite based on poly(m-phenylenevinylene-co-2, 5-dioctoxy-p-phenlenevinylene)," *Proceedings of the ICSM*, Wollongong, Australia (2004)

5. Avadhanula, W. Wondmagegn, M. Kandadai, D. Zhang and S. A. Curran, "New Polymer Nanotube Design from Graft Polymerization," H. Kuzmany, J. Fink, M. Mehring, and S. Roth, eds., *Kirchberg Proceedings* (2005)

6. Avadhanula, Aditya; Wondmagegn, Wudyalew; Kandadai, Madhuvanthi; Zhang, Donghui; Curran, Seamus A., "Meso-structure formation for enhanced organic photovoltaic cells," *XIX International Winterschool/Euroconference on Electronic Properties of Novel Materials. AIP Conference Proceedings*, Volume 786, pp. 224-227 (2005).

7. One patent application

Seamus A. Curran, James L. Dewald, Amanda V. Ellis and Wudyalew T. Wondmagegn, *Fabrication of a Gold-Polymeric Nanocomposite. Serial No. 11-166,606*

2. BACKGROUND THEORY OF CHARGE TRANSPORT AND SCHOTTKY EFFECT

2.1 Nature of charge carriers in organic semiconductors

In the electronic structure of organic polymers, there is a large energy difference between the highest occupied molecular orbital (HOMO) and the lowest unoccupied molecular orbital (LUMO). This implies it is an electrically insulating material [61]. Like an atomic orbital, a molecular orbital can be occupied by no more than two electrons. When a covalent bond is formed, the two electrons originally in the atomic orbitals of the separate atoms now go into a much lower energy bonding MO. The formation of a covalent bond involves the sharing of only two electrons. Those electrons form the pair that can be accommodated in the bonding molecular orbital. Two different geometries are possible [260]. The bonding MOs that result in a geometry cylindrically symmetrical about a line joining the two nuclei involved are called sigma (σ) orbitals, and the bonds formed are called σ-bonds (cf. Fig. 2.1 (a)}.

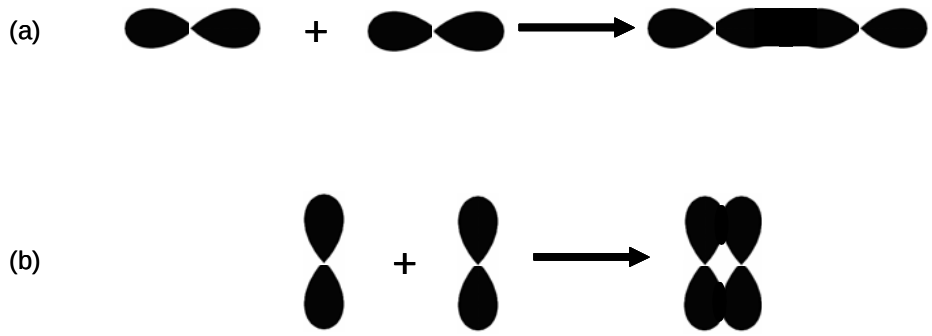

Fig 2.1 (a) Overlap of two p atomic orbitals to give a bonding σ MO. (b) Overlap of two p atomic orbitals to give a bonding π MO.

Another type of bonding MO and, therefore, a second type of covalent bond, can be formed by the overlap of two atomic 2p orbitals as shown in Fig. 2.1 (b). This bonding MO is not cylindrically symmetrical about a line joining the two nuclei. It is called a pi (π) bonding molecular orbital. The resultant covalent bond is called a π-bond.

The arrangement of the electrons in the outer most level of carbon when carbon is covalently bonded is not the same as when carbon is in the atomic state. The electronic configuration of carbon in the atomic state is $1s^2\ 2s^2\ 2p^1_x\ 2p^1_y\ 2p^0_z$. From this configuration, it would be expected that carbon would form bonds by a combination or overlapping of the two partially filled p orbitals with s and p atomic orbitals of other atoms and thus that the combination with two hydrogen s atomic orbitals would lead to CH_2 . However, the stable hybrid of carbon is methane (CH_4). Furthermore, the four carbon-hydrogen bonds in CH_4 are equivalent. The equivalent bonding is achieved by hybridization of the one s and three p atomic orbitals in the second energy level to give four orbitals of a new type, which are called sp^3 orbitals. These orbitals are equivalent, and each contains one electron. The four sp^3 hybrid orbitals are directed to the corners of a tetrahedron [210]. The sp^2 hybrid orbitals of carbon occurs when it is bonded to three other atoms [210]. The carbon main chain of conjugated polymers consists of covalently bonded carbon atoms. Three of the four valence electron orbitals of the carbon atoms in the conjugated main chain, one s- and two p- atomic orbitals, are hybridized into three sp^2- orbitals [125],[223]. These orbitals form the so called σ-bonds to other carbons, hydrogen, or heteroatoms. The remaining valence electron is in a p_Z-orbital oriented perpendicular to the σ-bonds. The p_Z-orbitals interact with their neighbors, forming π- bonds between the carbons [61]. We note also that there is an other class of orbital hybridization for triple bond

carbons such as acetylene known as sp hybrid orbital [210]

2.1.1 Peierls Distortion

In organic conjugated polymers, the backbones consist of sp^2 hybridized carbons. This electron configuration results in three σ-bonding electrons, the 2s, $2p_X$, $2p_Y$ electrons, and a remaining $2p_Z$ electron. The p_Z-orbitals interact with their neighbors, forming π-bonds between the carbons. From an organic chemistry point of view, the macromolecule has alternating single and double bonds (σ-bonds and σ+π -bonds, respectively) along the main chain [61].

The solid state physicist will, however, view this a little differently. Since the inter-chain coupling in these systems is normally weak, the main chain is essentially a one dimensional lattice. Three of the valence electrons form bonds to the neighbors and leave one free electron per unit cell. In the electronic structure there is a half-filled energy band, characteristic of a metal. However, this material is not stable as a metal; a one dimensional system with a half-filled energy band is unstable and will undergo a transition to a dimerized state, leading to a gap at the Fermi energy [100]. This is a Peierls distortion which is a disorder-to-order transition or a metal-to-insulator transition. The energy gap separates the HOMO, which is the valence band, from the LUMO, which is conduction band.

The dimerization (metal-to-insulator transition) means that the unit cell will be twice as large as before and will contain two bonds, one long and one short, (Fig. 2.2). From the appearance of the energy gap in the energy band, we can now expect a semiconductor. In their pure state conjugated polymers are semiconductors or even insulators, with a band gap, E_g, between 1 and 4 eV [61]. Few of them are found in

the lower part of this energy range, and therefore, the intrinsic conductivities are low due to small thermal excitation across the band gap. The polymers are often colored since the band gap corresponds to photon energies in the visible region.

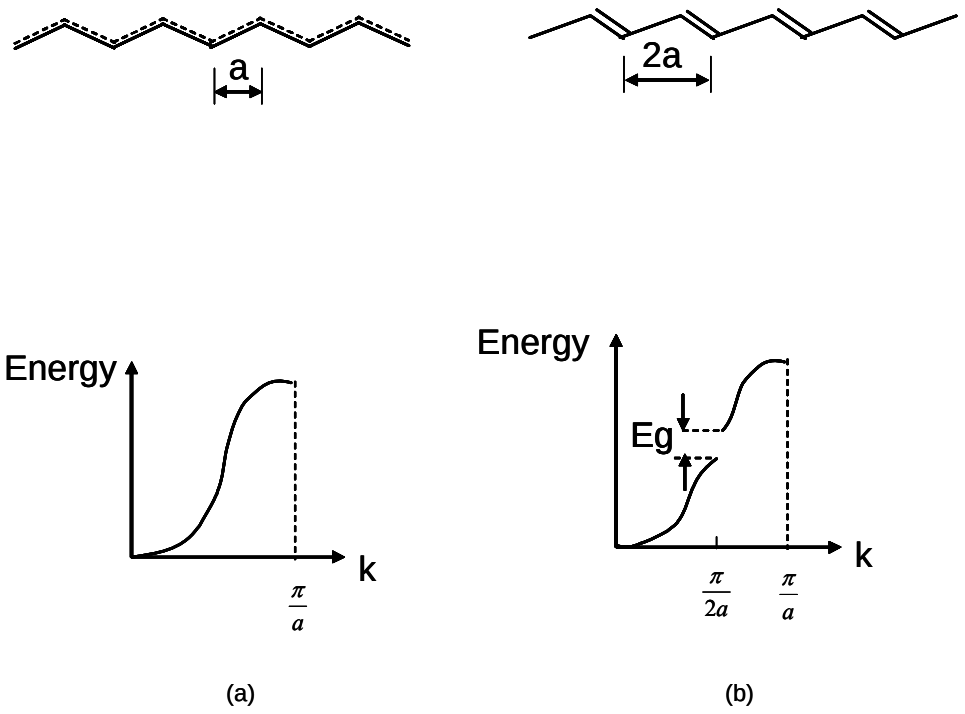

Fig 2.2 Process of transition from (a) metallic state to (b) non-metallic state by dimerization.

2.1.2 Elementary Excitations

The basic assumption of modern theory of condensed matter is that there exists a stable ground state and excited states of higher energy. In general, the energy of an excited state can be expressed as the sum of energies of elementary excitations or quasi-particles. Just as atoms, ions, and molecules are the building blocks of a crystal in the sense of structure, these elementary excitations are the building blocks of a solid in the sense of motion [143].

2.1.3 Solitons in polyacetylene

The conjugated polymer with the simplest structure is polyacetylene. It has only a main chain of alternating single and double bonds between carbon atoms, with one hydrogen atom attached to every carbon. Fig. 2.3 shows two degenerate ground states of trans-polyacetylene.

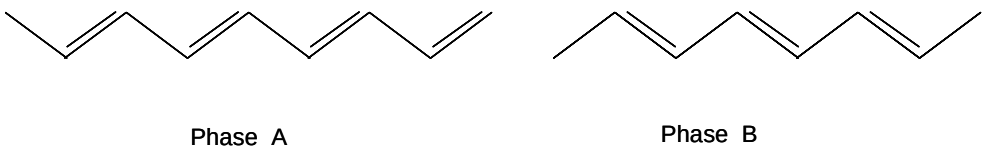

Fig 2.3 Degenerate ground states of trans-polyacetylene

Putting two such trans-polyacetylene chains together, a phase transition region will occur where the chain has an apparent bond alternation defect, see Fig. 2.4. This defect, called a soliton and often referred to as being a quasi-particle, corresponds to an unpaired electron and gives rise to a localized electronic state in the middle of the otherwise forbidden energy gap [87]. Apart from the neutral soliton, addition or withdrawal of an electron creates the charge and spin configurations as shown in Fig. 2.5.

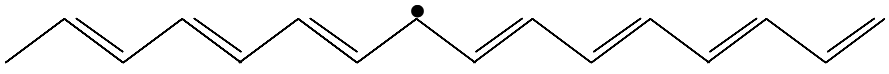

Fig 2.4 Creation of a soliton in trans-polyacetylene.

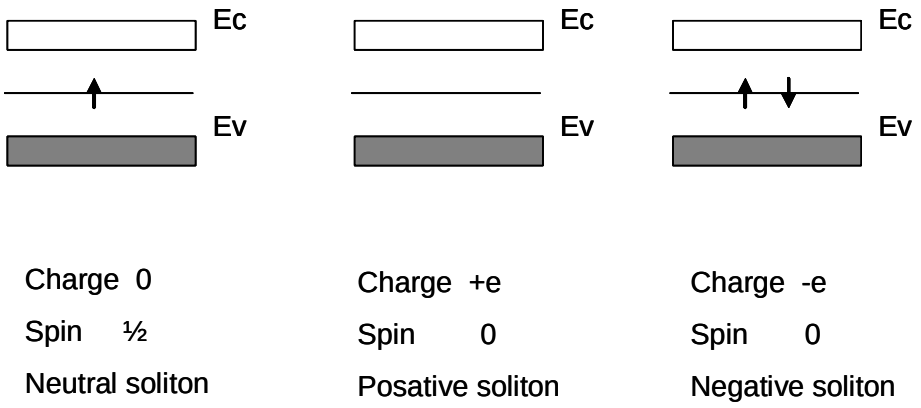

Fig 2.5 Charge and spin combinations for differently charged solitons.

2.1.4 Polarons and Bipolarons

The term polaron is known from inorganic semiconductors to describe an elementary excitation resulting from the effect of motion of an electron in an ionic crystal. In simple terms, an electron moving in an ionic crystal attracts the positive ions and repels the negative ones. Hence it polarizes its surroundings. The polarization field thus produced, in turn, affects the motion of the electron itself. This set of the moving electron and its accompanying polarization field is called a polaron [129].

Conjugated polymers can also be built from aromatic units. Pyrrole, thiophene, and benzene are examples of monomers from which non-degenerate ground state conjugated polymers can be synthesized. In these polymers there are two different possible bond alternations, since all carbon atoms are not in equivalent positions. This is synonymous with a non-degenerate ground state. The two different bond alternation patterns are referred to as aromatic and quinoidal. The aromatic form

is the lowest energy state. For instance, the left and the right sides of the soliton in polythiophene, as depicted in Fig. 2.6, have different energies.

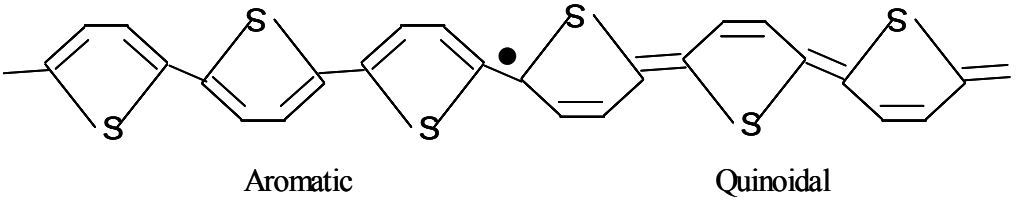

Fig 2.6 Soliton site in a polythiophene.

Contrary to solitons in polyacetylene, which are more stable and can be positioned anywhere in the chain, solitons in non-degenerate polymers are energetically unstable. They move along the chain, thereby changing the high energy quinoidal rings into low energy aromatic rings. If defects in non-degenerate ground state polymers are to be stable, bound stable defects must be created. This bound double-defect (quasi-particle) is called polaron if singly charged, Fig. 2.7(a) and bipolaron if doubly charged, Fig. 2.7(b) [87].

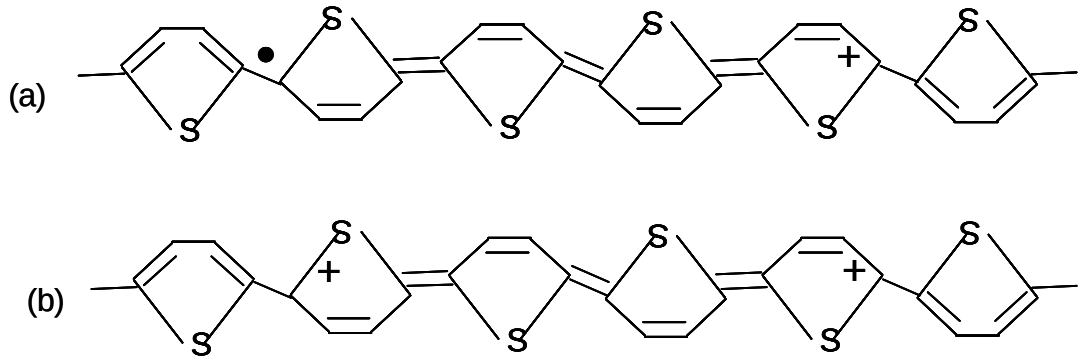

Fig 2.7 A polaron (a) and bipolaron (b) in polythiophene.

In the same way as solitons, which can be related to the polarons and bipolarons because a polaron can be regarded as a combination of a soliton and an antisoliton, the polaronic defects give rise to states in the band gap as shown in Fig. 2.8. These new states resulting from solitons, polarons, and bipolarons can be observed in optical absorption spectra [69][98][241] because new transitions become possible.

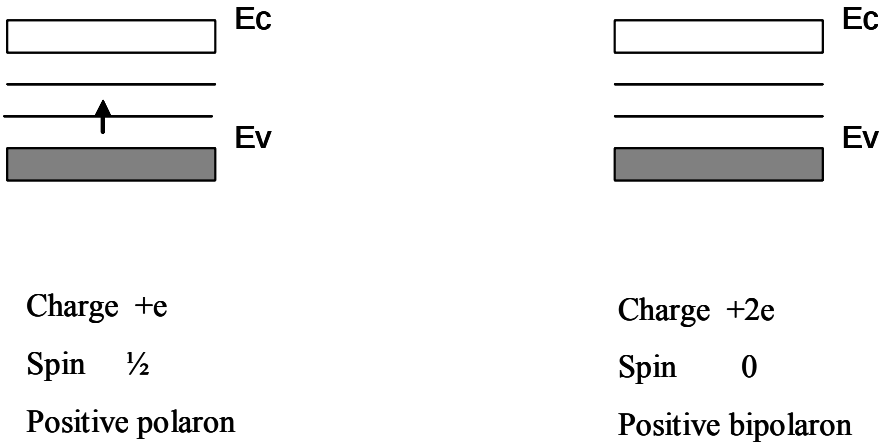

Fig 2.8 Energy band diagrams showing charged states of a non-degenerate ground state polymers.

2.2 Charge transport in conjugated polymers

The relation between drift velocity of electrons or holes in a solid material and an applied electric field is described in terms of Mobility. The mobility of polymeric semiconductor material is found to be very low and strongly electric-field and temperature dependent [11][21][71][94],[189]. In metals and conventional semiconductors, charge transport occurs in delocalized states, and is limited by the scattering of the carriers, mainly due to thermally induced lattice deformations

(phonons) [104]. Such a model is not valid in low conductivity materials such as amorphous or organic semiconductors. In these materials, transport occurs by the hopping of charges between localized states.

The main difference between the delocalized and localized transport is that, in the former, the transport is limited by phonon scattering, whereas in the latter, it is phonon assisted. Accordingly, the charge mobility decreases with temperature in conventional crystalline semiconductors, the reverse being true in most organic materials. Several models have been developed to rationalize this hopping transport. Over the past decades intense research has been carried out in order to explain the transport of charge carriers in such materials, which would justify such low mobility. There are several transport models showing good agreement with the electrical measurements for some particular systems, but no complete solution is available due to the diversity and complexity of these systems. Here, we present the most common transport models found in the literature.

2.2.1 Hopping in a Disordered Medium

The absence of an ideal three dimensional periodic lattice structure in disordered polymer semiconductors made it impossible to describe the charge transport processes in terms of standard semiconductor models. Because of their spatial and energetically disordered configuration, these systems have no translation symmetry. The concept of band conduction by free charges does not apply. Instead, the formation of localized states is enhanced and a different theoretical approach is

required. In order to participate in the transport, the charge carriers must hop between these localized states (inter or intra-chain transitions). This hopping usually leads to a very low carrier mobility. To overcome the energy difference between two localized states, the carriers absorb or emit phonons. This process of phonon-induced hopping was suggested by Conwell [39] and Mott [164] in connection with metallic conduction in inorganic semiconductors, and later by Pines, Abrahams and Anderson [187] for electron relaxation processes in silicon. Mott discusses the hopping transport in a constant density of states (DOS), in which he argues that the hopping over long distances and the hopping to high energy states are equally important [132].

Later, Miller and Abrahams proposed a hopping model based on a single-phonon jump rate description [117]. Their evaluation was made in the case of a lightly doped semiconductor at a very low temperature. The localized states were shallow impurity levels. The energy of these levels sits in a narrow range, so the probability for an electron on one site to find a phonon to jump to the nearest site is high.

The model of variable-range hopping, based on the Miller–Abrahams equation for the hopping rate, is commonly accepted as an adequate, although simple, approach to the problem of charge transport in disordered organic materials [8][11][158]. It suggests that the average hopping rate and the mobility are controlled by carrier jumps from deeper states to shallower states. Most charge carriers in deeper states are localized under equilibrium conditions and do not contribute to transport. On the other hand charge carriers in shallower states play a major role in transport.

The jump probability exponentially decreases with the distance and energy difference between starting and target sites. Thus a carrier will most probably jump to a site that corresponds to a trade off between the distance and energy difference. This combination depends upon the temperature, the carrier localization radius, and the DOS distribution.

Charge transport in many doped organic materials shows a strong relationship to the external electric field *E* and temperature *T*. The field dependence of the mobility is well described by Gill's empirical law, $log\mu \propto \sqrt{E}$, over a wide range of field strength and for various combinations of the dopant molecules and host materials [83][213]. This dependence is recognized as the Pool-Frenkel law [59][77]

$$\mu = \mu_0 \exp\left[\frac{-\Delta}{kT}\right]\exp\left[\gamma\sqrt{E}\right] \tag{2.1}$$

$$\gamma = B\left[\frac{1}{kT}-\frac{1}{kT_0}\right] \tag{2.2}$$

where B ≈ $4x10^{-4}$ $(e^2$ V cm$)^{1/2}$, and *To* ≈ 500 ^{0}K. Except for the compensation factor (*1/kTo*), expressions (2.1) and (2.2) describe the Arrhenius dependence of the mobility, which arises if moving charges must hop over a Coulomb barrier of height Δ in energy. The exponential dependence of μ on $\sqrt{E}$ universally observed in molecularly doped polymers arises naturally from slowly varying spatial fluctuations in the potential energy of a charge migrating through the material [173]. Such energetic fluctuations can arise from a random distribution of molecules in the medium possessing permanent electric dipole moments [60].

2.2.2 The Polaron Model

In the case of long conjugated polymers, with a delocalized-electron structure, the main transport path is known to be intramolecular and the charge carriers are polaronic: this is reflected in the high electrical anisotropy seen for stretched materials [66][101]. This transport mechanism is not the case for films made from oligomers, where transport orthogonal to the long molecular axis could dominate; it has been shown that for PPV the film morphology strongly influences the transport properties, indicating that intramolecular interactions are not sufficient to explain experiments [64].

The polaron model was first introduced in the case of inorganic crystals, and has later been used to explain the charge transport in molecular crystals and conjugated polymers [99],[159][160][178]. This transport model takes into account the strong electron phonon interaction. A polaron is basically a quasiparticle which results from the combination of a charge carrier with a lattice deformation induced by its charge. In polaronic charge transport, not only does the charge move under an applied electric field, but the lattice deformation moves with it. Typically, for hopping transport of polarons, a description in terms of Miller-Abrahams hopping [158] is insufficient, as multiphonon hopping rates need to be considered [65][101]. The charges moving by thermally activated hops between adjacent sites have a mobility which is field (E) and temperature (T) dependent [147][148]:

$$\mu = \mu_0 \exp\left[-\frac{E_r}{4kT} - \frac{(aE)^2}{4E_r kT}\right] \frac{\sinh(aE/2kT)}{aE/2kT} \tag{2.3}$$

where μ_0 is slightly temperature dependent. However, using the Marcus theory, the polaron contribution to the activation of the mobility is insignificant. The activation of the mobility using this model amounts to 25-75 meV [213], while using the disordered model the activation energy amounts to 420 meV [11],[72].

Another model that takes into account the strong coupling of charge carriers with the lattice is Su-Schrieffer-Heeger (SSH) theory [233], which describes the electronic structure of conjugated polymers. This model is based on the concept of bond alteration along a perfect conjugated polymer chain with weak interchain coupling. Adding a charge to the polymer chain leads to a profound change in its geometrical structure, characterized by a permutation of the bond alteration over a certain number (approximately $3 - 5$) monomeric units. The π-electrons are treated in a tight-binding approximation. The main omission of the SSH model is that it does not consider the electron-electron and electron-hole interactions, which play an important role in the transport and recombination of charge carriers.

2.2.3 Hopping in a disordered medium including polarons

Both the disorder and polaron models discussed above predict the mobility is temperature and field activated but differ as to the functional dependencies [20]. It was demonstrated [7],[12],[66],[146][180] that the interplay between the polaronic and disorder effects may be responsible for the specific temperature dependence observed in some amorphous materials.

Considerable debate continues regarding the nature of charge carriers in

molecularly doped polymers (MDP's) [20][58],[120],[206][228] and other organic solids of current technological interest [205],[208][261]. Experiments clearly show strong thermal activation of the field dependent mobility μ, that could arise equally well from a carrier's interaction with phonons (polaron binding), or from static properties of the material (energetic and spatial disorder).

Many recent studies of a wide range of molecularly doped polymers (MDP's) and conjugated main chain and pendant-group polymers, as well as vapor-deposited molecular glasses, have been described within the framework of Bässler's Gaussian disorder model [70]. The underlying idea behind the Gaussian disorder model (GDM) of Bässler is that the activated mobilities arise from carriers hopping through a Gaussian density of transport states of energetic width σ(0.1 eV), via Miller-Abrahams hopping rates [20][180]. Multiphonon processes typical of polaron transport are absent in such a model.

However, some people, by contrast, assumed carriers to be polarons moving in a disordered medium [58][228]. Whether charge carriers are polaronic or bare is also of obvious importance to ordered organics (crystals), where careful quantitative analysis [120] for naphthalene [205] has shown that the assumption of bare carriers leads to inconsistencies that are avoided when strong carrier interactions with phonons are included. Recently, experimental and theoretical characterization of the correlated, dipolar nature of the disorder through which carriers move in MDP's has been shown using the idea that mobilities of MDP's are entirely compatible with small polaron motion in a random energy landscape, provided it has the spatial

correlations of the charge-dipole type [60][172][173][87-89]. An analytical disordered polaron model was suggested by Kenkre and Dunlap [58][71][121] to account for the polaron transport under the influence of energetic disorder. The drawback of their approach is that it requires unacceptably large values of intersite transfer integrals and polaron binding energy. However recent computer simulations by Parris [180] have demonstrated that the problem related to physical parameters can be solved assuming the small-polaron transport occurs in the presence of correlated energetic disorder.

2.3 Theory of rectifying metal semiconductor contacts

Metal-Semiconductor contacts form interfaces that give basic features of many metal-semiconductor devices such as rectifiers, field-effect transistors, and other surface junction devices. Although our knowledge of Metal-Semiconductor (MS) contacts can be traced as far back as early work by Braun (1874), it was not until 1938 that both Schottky and Mott independently suggested a model for the rectification mechanism. They pointed out that the observed direction of rectification could be explained by assuming that electrons passed over a potential barrier through the normal process of drift and diffusion. The barrier between the metal and the semiconductor can be identified on an energy band diagram.

2.3.1 Energy band bending of Metal-Semiconductor contact

To construct the band bending diagram of an MS contact, we first consider the energy band diagram of the metal and the semiconductor, and align them using the

same vacuum level. When a metal is placed in intimate contact with a semiconductor, the Fermi levels in the two materials must be coincident at thermal equilibrium [238]. However, the Fermi energies of the metal and the semiconductor do not change right away. This yields the flat band diagram. The junction is the place where the exciton dissociates [19]. Depending on the work functions of the metal and semiconductor, the MS contacts may be either ohmic or rectifying.

The case of rectifying (Schottky) behavior for the contact between a metal and an n-type semiconductor is illustrated in Fig. 2.9. In the figure, ϕ_m is the ionization potential of the metal in a vacuum and ϕ_s is the ionization potential of the semiconductor. The nature of the contact depends on the relative height of the Fermi levels ϕ_m and ϕ_s. Fig. 2.9(a) shows energy levels of a metal and n-type semiconductors before contact and Fig. 2.9 (b) shows anbiased band structure of a metal and n-type semiconductor after contact [254]

The barrier height, $q\phi_{bn}$, is defined as the potential difference between the Fermi energy of the metal and the band edge where the majority carriers reside.

$$q\phi_{bn} = q\phi_m - q\chi_s \tag{2.4}$$

In (2.4) $q\phi_m$ is the work function of the metal and $q\chi_s$ is electron affinity of the semiconductor. Electron affinity is expressed as

$$q\chi_s = q\phi_s - (E_c - E_F) \tag{2.5}$$

where

$q\phi_s$ = work function of the semiconductor, in eV

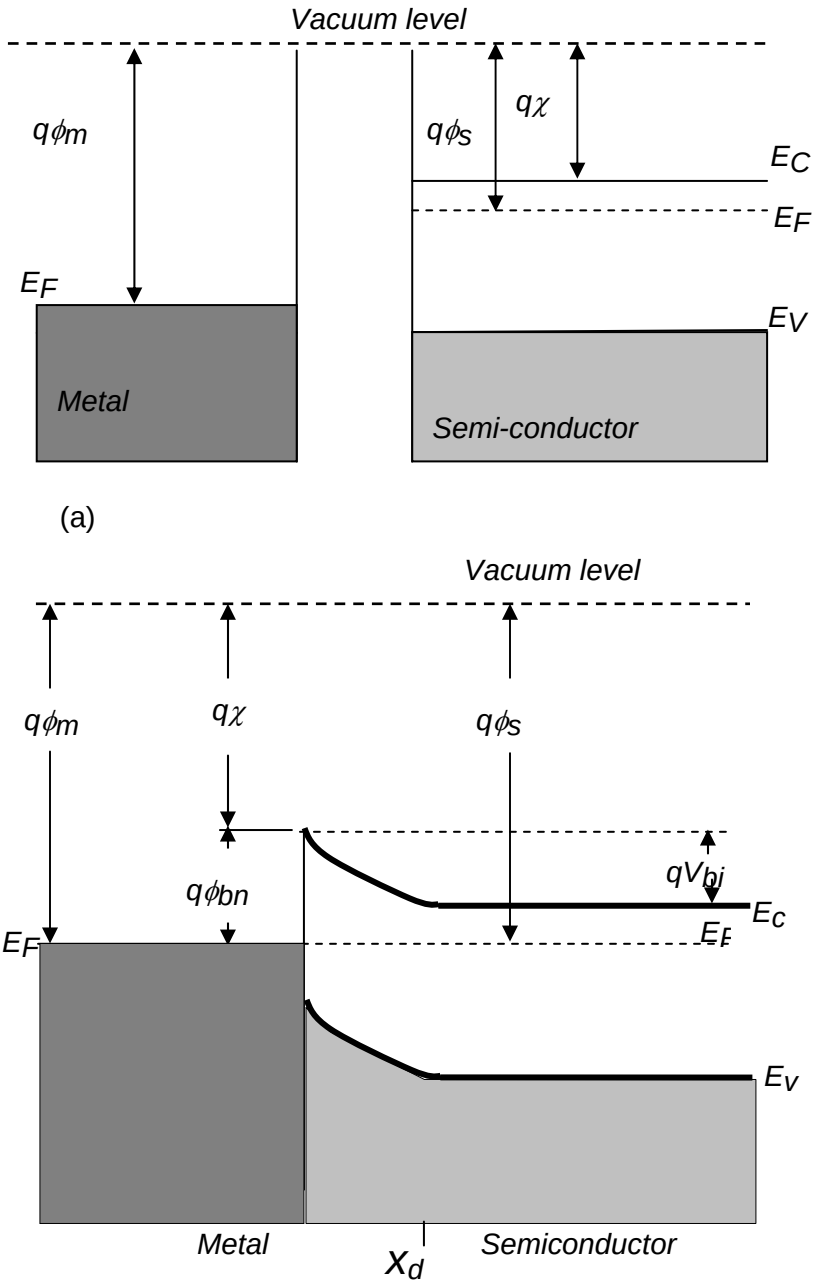

Fig 2.9 Energy levels of a metal-n-type semiconductor (a) before and (b) after contact

E_c = conduction band energy, in eV

E_F = Fermi energy level, in eV

The barrier encountered by electrons in the metal is $q\phi_{bn}$ whereas the built-in potential, qV_{bi}, encountered by electrons in the semiconductor, is given by:

$$qV_{bi} = q(\phi_m - \phi_s) = q\phi_{bn} - (E_c - E_F) \tag{2.6}$$

This theory assumes ideal conditions where dipole surface contributions to the barrier height and the electron affinity are thought to be unchanged when the metal and the semiconductor are brought into contact. It also assumes that there are no chemical reactions or physical strains created between the two when they are brought into contact. In practice, however, surface dipole layers do arise. This is because at the surface of a solid the atoms have neighbors on one side only. This causes a distortion of the electron cloud which belongs to the surface atoms, so that the centers of the positive and negative charge do not coincide.

The ideal metal-semiconductor theory assumes that both materials are infinitely pure and there is no interaction between the two materials. This theory also assumes no interfacial layer between the materials. In reality, the barrier height is altered by chemical reactions between the metal and the semiconductor, interface states at the surface of the semiconductor, and interfacial layers. The surface states are continuously distributed in energy within the forbidden gap and are characterized by a neutral level. Some general trends however can be observed. As predicted by (2.4), the barrier height at *n*-type semiconductors increases for metals with a higher work function, as can be verified for silicon. Gallium arsenide, on the other hand, is

known to have a large density of surface states so that the barrier height becomes virtually independent of the metal. Furthermore, one finds the barrier heights reported in the literature to vary widely due to different surface cleaning procedures.

In practice, due to chemical cleaning of the semiconductor, there is a thin oxide layer between the metal and the semiconductor. The charge in the surface states together with its image charge on the surface of the metal will form a dipole layer. This dipole layer will alter the potential difference between the semiconductor and the metal. Thus the modification to the Schottky-Mott theory is expressed as follows [197]:

$$q\phi_{bn} = \gamma(q\phi_m - q\chi_s) + (1 - \gamma)(E_g - q\phi_0) \tag{2.7}$$

where

E_g = bandgap of the semiconductor, in eV

$q\phi_0$ = position of neutral level (measured from the top of the valence band) and,

$$\gamma = \varepsilon_i / (\varepsilon_i + q\delta D_s) \tag{2.8}$$

where

ε_i = permittivity of oxide layer

δ = thickness of oxide layer

D_s = density of surface states

Hence if there are no surface states, $D_s = 0$ and $\gamma = 1$ and (2.7) becomes identical to (2.4) (the original Schottky-Mott approximation). But if the density of states is very high, γ becomes very small and $q\phi_{bn}$ approaches the value $(E_g - q\phi_0)$. This change in γ

is because a very small deviation from the Fermi level from the neutral level can produce a large dipole moment [197][198]. When this occurs, the Fermi level is said to be "pinned" relative to the band edges by the surface states.

Barrier Lowering due to Image Force Effects

The application of an electric field causes an image-force-induced lowering of the potential energy for charge carrier emission [238]. Consider a charge, in a vacuum, at a distance x from a metal surface. An opposite charge will be induced on the metal at a distance $-x$ from its surface. This image charge will give rise to an attractive force between the two, known as the image force, as described by (2.9). This force has associated with it an image potential energy which corresponds to the potential energy of an electron at a distance x from the metal. When an external field, E_{ext}, is applied, this image potential has the effect of lowering the Schottky barrier. Thus at high fields, the Schottky barrier is considerably lowered as shown in

$$E_{im}(x) = \frac{q}{4\pi\varepsilon_s (2x)^2} \tag{2.9}$$

The dielectric constant ε_s may not be the static dielectric constant. It depends on the characteristic of the electron residing on the near-surface region. The amount of barrier reduction due to the induced-image-force, $\Delta\phi_{im}$ is given by [142][238]

$$\Delta\phi_{im} = \sqrt{\frac{qE_{\max}}{4\pi\varepsilon_s}} \tag{2.10}$$

where E_{max} is the field near the interface, (x=0), which is assumed to have a constant

value in the absence of image-force effects.

In Fig. 2.10, the dashed line is the image potential ϕ_{im} (right abscissa) experienced by a positive charge carrier. The bold solid line ($\phi_{tot}=\phi+\phi_{im}$, left abscissa) shows the influence of the image force on a linear potential (ϕ, solid line, left abscissa). The linear potential is the gradient of the opposite sign the charge trapped in the boundary. Note that the zero point for ϕ_{im} is shifted up relative to that for ϕ and ϕ_{tot}. The image-force reduces the maximum potential by $\Delta\phi_{im}$ and shifts it away from the interface by x_{max}.

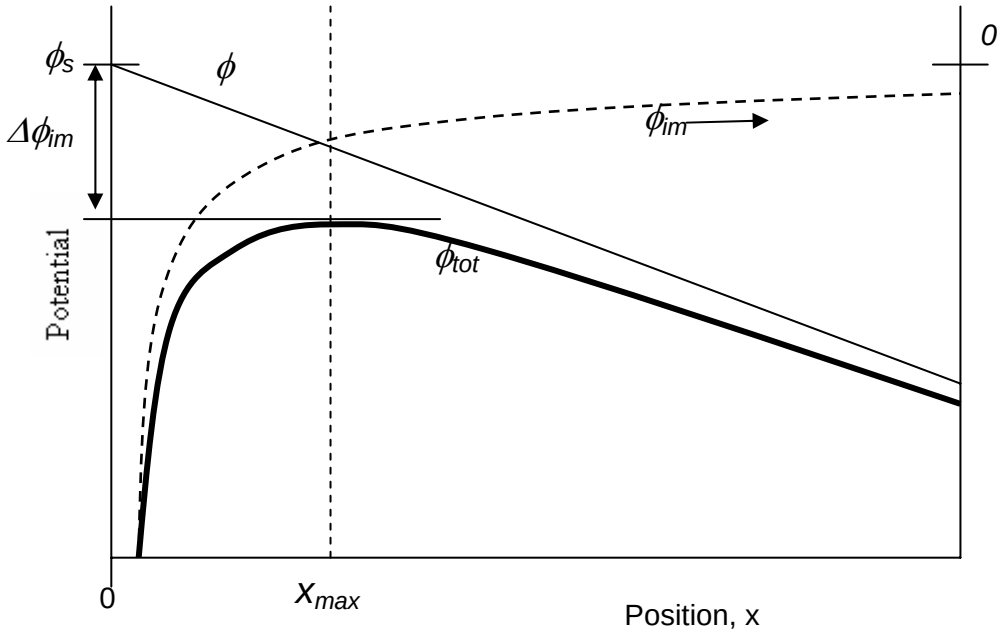

Fig 2.10 Schematic of barrier lowering caused by the image force effect.

2.3.2 Current transport mechanisms in the Schottky diode

The current across a metal-semiconductor junction is mainly due to majority carriers. Here we present the basic theoretical and semi-empirical physical concepts used to describe the transport properties of conjugated polymer-metal interfaces, basic definitions follow [238].

In the charge transport across Metal-Semiconductor junction, different charge transport mechanisms exist. These are: Thermionic emission, Generation recombination, quantum mechanical tunneling, and leakage currents.

a) Thermionic emission current

The current transport through the device by emission over the barrier is essentially a two step process. First, the electrons have to be transported through the depletion region, and this is determined by the usual mechanisms of diffusion and drift. Secondly, they must undergo emission over the barrier into the metal, and this is controlled by the number of electrons that impinge on the metal per second. This mode of current transport is commonly referred to as the "thermionic emission" current [56][177]. Diffusion theory assumes that the driving force is distributed over the length of the depletion layer. The analysis reveals that the thermionic emission currents can be written in the following form:

$$J = J_s\left(\exp(\frac{qV}{nkT}) - 1\right) \tag{2.11}$$

$$J_s = A^* T^2 \exp(\frac{q\phi_{bn}}{kT}) \tag{2.12}$$

$$A^* = \frac{4\pi q m^* k^2}{h^3} \tag{2.13}$$

where J is the current density, Js is the saturation current density, q is the absolute electron charge, m^* is the effective electron mass, h is Planck's constant, k is Boltzmann's constant, T is the absolute temperature, ϕ_{bn} is the barrier height, and n is the ideality factor which takes into account corrections to the original simple model, for example, image force barrier lowering. The Modified Richardson's constant (A^*) is calculated to be 120 $A^2/ K^2 m^2$.

The ideality factor, n, in (2.11) gives a measure of the quality of the junction which is highly process dependent. For an ideal Schottky junction, $n = 1$. In practice, however, larger values are obtained due to the presence of non-ideal effects or components to the current through the junction.

However, in real Schottky contacts, an ideal behavior deviation is frequently observed and the *I–V* curves deviate from equation (2.11). The Schottky effect, series resistance, the presence of other transport mechanisms [188], and inhomogeneous Schottky barrier heights [40],[116][176] have been confirmed by several authors as the most important causes of nonideal behavior.

b) Generation-Recombination Effects

For wide-band-gap materials, such as organic semiconductors, carrier

generation by thermal excitation across the gap is very small and usually neglected in calculations [254]. This is particularly significant at moderately low temperatures (175K to 235K). The current contribution, I_{gr}, due to the generation-reombination mechanism can be represented by [56],[254]:

$$I_{gr} = I_{gr0}\left[\exp\left(\frac{qV}{2k_BT}\right)-1\right] \tag{2.14}$$

where,

I_{gr0} is the saturation value of the generation-recombination component of the current I_{gr} .

$$I_{gr0} = \frac{qAwn_i}{2\,\tau} \tag{2.15}$$

where,

w is the depletion width, n_i is the intrinsic carrier concentration, A is the area of the depletion width, and τ is the effective carrier lifetime in the depletion region.

c) Current due to Quantum Mechanical Tunneling

Quantum-mechanical tunneling through the barrier takes into account the wave-nature of electrons, allowing them to penetrate through thin barriers. For a moderately to heavily doped semiconductor or, for operation at low temperatures, the current due to quantum mechanical tunneling of carriers through the barrier may become the dominant transport process [46],[177]. Except at very low biases, the

tunneling current in inorganic metal-semiconductor contacts can be represented by [211],[254]:

$$I_{Tn} = I_{Tn0}\left[\exp\left(\frac{qV}{E_0}\right) - 1\right] \tag{2.16}$$

where,

I_{Tn0} = tunneling saturation current

E_0 = tunneling constant

The tunneling saturation current is a complicated function of temperature, barrier height and semiconductor parameters. The tunneling constant *Eo* is given by [177]:

$$E_0 = E_{00}\coth\left(\frac{E_{00}}{kT}\right) \tag{2.17}$$

where,

E_{00} = a tunneling parameter inherently related to material properties of the semiconductor

d) Leakage Current

The leakage current, I_{lk}, is another parallel component of the total current. It is caused by surface leakage and can usually be significantly reduced by various designs and fabrication techniques. In practice, it is the component which appears to by-pass the metal/semiconductor interface and is often thought of as a large leakage resistor, $R_{lk,}$ in parallel to it. Thus the leakage current can be expressed as:

$$I_{lk} = V / R_{lk} \tag{2.18}$$

In a given junction, a combination of all transport mechanisms could exist. However, typically one finds that only one mechanism determines the current.

3. LITERATURE REVIEW OF RESEARCH ADVANCES AND CHALLENGES IN THE REALIZATION OF ORGANIC ELECTRONIC AND PHOTONIC DEVICES.

In this chapter we present the literature review of the three different device applications of organic semiconductors and metal semiconductor junctions. When used as a rectifier, a metal-semiconductor junction is called a semiconductor diode. As a light source, it is a light emitting diode or LED, and when used as a photoelectric energy converter, it is often called a solar cell. In addition to OLEDs and solar cells, there are great research advances towards the realization of organic field effect transistors.

3.1 Photovoltaics

A photovoltaic cell (solar cell) is a device, which converts incident light to electrical energy. The most common form of solar cells are based on the photovoltaic (PV) effect in which light falling on a two layer semi-conductor device produces a photo-voltage or potential difference between the layers. This voltage is capable of driving a current through an external circuit and thereby producing useful work.

The conversion efficiency of a photovoltaic (PV) cell is the proportion of sunlight energy that the cell converts to electrical energy. The efficiency of solar cells is affected by a variety of factors such as absorption of solar radiation, generation of electron - hole pairs, and separation of electrons from holes. Improving this efficiency

is vital to making PV energy competitive with more traditional sources of energy.

Absorber materials should be of sufficient band gap to absorb radiation within the UV and visible range of the solar spectrum. Unit absorptance, i.e., the ratio of the total absorbed flux to the incident flux is ideal, but in practice this is lower than 1. The limit of efficiency is first determined by the amount of solar radiation which is incident on the cell but cannot be absorbed. Only photons with energy greater than or equal to the band gap of the material can excite an electron from valence band to conduction band. All those photons with energy smaller than the band gap are just transmitted through and do not count towards the generation of electron-hole pairs (EHPs) in the device. Those photons with energies greater than the band gap can only generate one electron.

It is not sufficient to just create electron-hole pairs, since these will recombine radiatively at the first possible opportunity. It is necessary to move the electron away from the hole and to ensure that the two do not recombine. For this to happen, some mechanism must provide a force equal to or greater than the Coulombic attraction force between the electron and the hole, such that it will be preferable for the electron to stay away from the hole, or even to move away from it. If such a force doesn't exist, the electron and hole will recombine radiatively. Such emission may be observed as photoluminescence. In polymers, the formed electron-hole pair bound by Coulombic forces is called an exciton, and may be split at defects or interfaces with other materials.

The most common configuration of photovoltaic device (the first generation photovoltaic) consists of a large-area single layer p-n junction diode, which is capable of generating usable electrical energy from light sources with the wavelengths of solar light. These cells are typically made using silicon.

However, successive generations of photovoltaic cells are currently being developed that may improve the photo-conversion efficiency for future photovoltaic. The second generation of photovoltaic materials is based on multiple layers of p-n junction diodes. Each layer is designed to absorb a successively longer wavelength of light (lower energy), thus absorbing more of the solar spectrum and increasing the amount of electrical energy produced. The third generation of photovoltaic is very different from the other two, and is broadly defined as a semiconductor device which does not rely on a traditional p-n junction to separate photo-generated charge carriers. These new devices include dye sensitized cells, organic polymer cells, and quantum dot solar cells [151]. The third-generation is used to describe different types of research in different contexts. It is research into thin-film photovoltaic devices involving abundant, non-toxic and durable materials where the energy conversion efficiency potential is higher than that possible from the standard single-energy-threshold conversion process. While the thermodynamic limit of the efficiency of the standard photovoltaic conversion process is 33%, the corresponding limit for a third generation approach can be as high as 93% [150].

3.1.1 Photovoltaic technologies

3.1.1.1 Single-crystal and polycrystalline silicon solar cells

Single-crystal silicon cells are sliced from single-crystal boules of grown silicon, these wafers/cells are now cut as thin as 200 microns. Efficiency of a solar cell made of single-crystal silicon is about 24 % (laboratory) and 14 to 17 % (production) [89].

Polycrystalline cells are made from similar silicon material except that instead of being grown into a single crystal, it is melted and poured into a mold. This forms a square block that can be cut into square wafers with less waste of space or material than round single-crystal wafers. As the material cools it crystallizes in an imperfect manner, forming random crystal boundaries. The efficiency of energy conversion is slightly lower. The efficiency of a solar cell made of polycrystalline silicon is about 18 % in the laboratory and 13 to 17 % in production [90].

3.1.1.2 Thin film solar cells

Crystalline silicon is often referred to as the first generation photovoltaic technology, while the second generation photovoltaics consists of thin film solar cell materials such as amorphous silicon (a-Si), cadmium telluride (CdTe), copper indium gallium diselenide (CIGS), and thin film crystalline silicon. The driving force for the development of thin film solar cells has been their potential for the reduction of manufacturing costs [166]. While silicon solar panels are assembled from individual

cells processed from about 100 cm^2 silicon wafers, thin film semiconductor materials can be deposited onto large surfaces, which is beneficial for volume production. Also, as direct band gap semiconductors, thin film semiconductor materials have a much higher absorption coefficient than silicon. Therefore a semiconductor layer that istypically less than 1 μm thick is required, which is 100-1000 times thinner than for Si. The amount of expensive semiconductor material is thus reduced. Alternately, more expensive semiconductors can be used in thin films. A thin-film polycrystalline material, which has reached a research efficiency of 17.7%, delivers the highest completed module efficiency for full sized power modules [16].

3.1.1.3 III-V Semiconductors

Semiconductors such as GaAs, GaAlAs, GaInAsP, InAs, InSb, and InP are interesting solar cell materials because they have near-optimal band gaps. These materials are extremely expensive, and have found applications only in space solar cells, where performance is a more important criteria than cost. The high cost of the cells, including materials, manufacturing and processing costs, hinders the application of these technologies to terrestrial applications. However, III-V materials constitute the basis of the highest efficient cells.

A three junction tandem cell, which is mechanically stacked (InGaP/GaAs/InGaAs), has been recently developed by Japan Energy Co, Sumitomo Co., and Toyota Technological Institute, achieving 33.3% efficiency [240]. Tandem cells or multiple junction cells are designed in such a way that part of the incident

light is not absorbed at the top cell, but passes through it and is utilized by the bottom device [119]. This allows using the solar spectrum more effectively, and increased efficiencies can be obtained. Several approaches such as the two-terminal tandem, three-terminal cascade cell or the four terminal connection cell have been successfully employed, obtaining efficiencies above 30%. Under 1 sun irradiance, a single solar cell only converts 30% of the solar energy. But a tandem structure of two cells can convert 42% and a tandem structure of three cells can convert 49% [53].

3.1.1.4 Dye-sensitized nanostructured solar cells

Dye-sensitization dates back to the 19th century, when photography was invented. However, the use of dye-sensitization in photovoltaics remained unsuccessful until a breakthrough at the early 1990's. By the successful combination of nanostructured electrodes and efficient charge injection dyes, solar cells with energy conversion efficiency of 7% and 10% were developed in 1991 and 1993 respectively [128],[174]. This solar cell is called the dye sensitized nanostructured solar. In contrast to the all-solid conventional semiconductor solar cells, the dye-sensitized solar cell is a photoelectrochemical solar cell i.e. it uses a liquid electrolyte or other ion-conducting phase as a charge transport medium. Due to the high efficiencies and long-term stability reported for the dye-sensitized solar cells, research interest in this technology grew rapidly during the 1990's.

3.1.1.5 Conductive polymers

Organic-based solar cells have high potential to reduce the cost of photovoltaics. Low-cost active materials, high-throughput reel-to-reel deposition technologies, and application versatility makes them very likely to become competitive against inorganic thin-film devices. However the power conversion efficiency of organic photovoltaics (OPV) is still too low.

While photovoltaic cells consisting of a single layer of conjugated polymer in general exhibit low efficiency of energy conversion [232], blends and heterojunctions with materials having high electron affinity considerably enhance not only the photon-to-current efficiency but also the more important power conversion efficiency [24][183].

Single Layer Cell

Single layer structures consist of only one semiconductor material between metal electrodes of asymmetrical work functions (usually ITO and Al) and are often referred to as Schottky type devices or Schottky diodes since charge separation occurs at the rectifying (Schottky) junction with one electrode. The other electrode is supposed to be ohmic nature. Under forward bias, holes from the high work function metal and electrons from the low work function metal are injected into a thin film of a single-component organic semiconductor. Forward bias currents are orders of magnitude larger than reverse bias currents at low voltages. The rectifying diode characteristics can be accompanied by radiative recombination channels of the

injected electrons and holes within the molecular solid; the result is an LED. If photon-induced free charge carrier generation is allowed at the same time, the device emits light under forward bias and exhibits a significant photocurrent under a reverse bias field. This shows that this rectifying junction has a dual function.

The single layer structure is simple, but absorption covering the entire visible range is rare using a single type of molecules. The photoactive region is often very thin and since both positive and negative photoexcited charges travel through the same material, recombination losses are generally high and efficiency low. The high exciton binding energy (200-500 meV) in most organic materials [92][250] is also another debilitating factor of efficiency. Higher efficiencies can be achieved if a heterojunction between hole and electron accepting polymers is incorporated. Bilayer [88] or blend structures [27] have better efficiency than single layer structure cells.

Bilayer Device

Conjugated polymer/fullerene plastic solar cells of the first generation were consisted of two distinct layers, made of a donor polymer and an acceptor fullerene [24], respectively, sandwiched between two metal contacts. Carbon nanotubes are important organic materials for nanotube/polymer bilayer solar cells [131]. This structure benefits from the separated charge transport layers that ensure connectivity with the correct electrode, and give the separated charge carriers only little chance to recombine with its counterpart. The drawback is the small interface that allows only excitons of a thin layer to reach it and get dissociated.

The highest efficiencies for pure polymer-based solar cells were reported for bilayer devices produced either by laminating a polythiophene derivative (POPT) with a cyano-substituted poly(*p*-phenylenevinylene) (MEH-CN-PPV) as the electron acceptor or with PPVs covered by a thin layer of a polybenzimidazobenzophenanthroline ladder polymers as the electron acceptor. These efficiencies were reported to be 1.9% [88] and 1.5 % [114] respectively.

Bulk Heterojunction Device

In organic solar cell structures, excitons are generated throughout the device; however, they typically diffuse only about 10nm [201] before decaying. Hence, only excitons created within this distance of the planar interface between donor and acceptor material split effectively into free charge carriers. This considerable limitation was solved by blending donor and acceptor material. By virtue of the mesoscopic morphology, this configuration can create a large interfacial area between donor and acceptor on length scales comparable to the exciton diffusion length [23]. The resulting interpenetrating donor-acceptor network is called a bulk heterojunction, because the heterojunction is distributed throughout the photovoltaic active volume.

By mixing the polymer and the fullerene components, thus replacing a single flat junction with an interpenetrating network bulk-heterojunction, the device efficiency was dramatically improved [200][214],[232]. The strong point of this structure is the large interface area. This structure requires the molecular mixing on a scale that allows good contact between alike molecules and most excitons to reach the

donor-aceptor (D/A) interface. The bulk-heterojunction principle relies on an active layer that consists of an intimate mixture of two different materials. One is serving as an electron donor and the other as an acceptor, sandwiched between two selective contacts. Inside the active layer a nanoscaled heterophase enables a very efficient charge generation throughout the bulk, resulting in nearly 100% efficiencies for converting absorbed photons to electrons [57],[207][253]. The active layer of the cell is constructed by blending a conjugated polymer donor and a high electron affinity acceptor such as fullerene [23],[25][95][268], polymer [95][96] and inorganic nanocrystal [84][91],[108].

It is an ongoing research challenge to realize the optimal morphology in which the phase separation is small enough to have efficient charge carrier separation. Research has also been focused on enhancing the efficiency of these cells through the use of new materials and device structures. PV cells employing polymerfullerene heterojunctions have been shown to have power conversion efficiencies approaching 5% [73][145]. A double-heterostructure copper phthalocyanine (CuPc)/C60 thin film cell with Ag as the metal cathode is reported to have an efficiency of 4% [263]. By stacking two such cells the efficiency has been further enhanced and yielded 5.5% [264].

The newly developed hybrid nanocrystal/polymer solar cell exhibits some advantages over previous cells [91]. The first advantage comes from the combination of the high electron mobility and stability of inorganic semiconductors and flexibility of polymers. The second advantage is the enlargement of the absorption which comes

from the compensated light harvest of nanocrystal and conjugated polymer [91].

In the hybrid nanocrystal/polymer solar cell, photoinduced charge separation is favored between high electron affinity inorganic semiconductors and relatively low ionization potential polymers. Upon irradiation, the conjugated polymer and nanocrystal both absorb the photons and produce excitons (electron-hole pairs). The excitons are separated into free charges at the interface of polymer and nanocrystal. The electrons from the excitons in the conjugated polymer transfer to nanocrystals, and the holes from the excitons in the nanocrystals transfer to the conjugated polymer. The separated electrons and holes move to cathode and anode, respectively, by their own pathways. This results in the formation of photocurrent and photovoltage.

So far, various hybrid polymer solar cells have been reported, using CdSe nanodots, nanorods [109], and tetrapods [236],[237], and using nanoparticles of TiO_2 [130], ZnO [14],[15], PbS [154],[258], PbSe [34],[191], $CuInS_2$ [6], and $CuInSe_2$ [5]. In a related approach, nanostructured TiO_2 has been filled with conjugated polymers [35],[36],[193]. In order to obtain hybrid polymer solar cells with high currents and fill factors, both electron and hole mobilities must be optimized. CdSe nanoparticles in poly[2-methoxy-5-(3′,7′-imethyloctyloxy)-1,4-phenylene vinylene] (MEH-PPV) initially showed external quantum efficiencies up to 12 % [91]. A major improvement came with the introduction of CdSe rods combined with poly(3-hexylthiophene) (P3HT) [109][110][150,166]. P3HT is a better hole transporting polymer and CdSe rods reduce the number of electron-hopping events between the nanocrystals needed

for transporting the electrons. Recent experiments demonstrate that CdSe tetrapods further improve the photovoltaic response because of their more favorable (perpendicular) orientation with respect to the plane of the film [236],[237].

The working principle behind organic bulk heterojunction (oBHJ) devices has typically been modeled employing the classical model of a metal-insulator-metal (MIM) device. In this model, the intimate mixture of electron-accepting and hole-accepting materials is treated as a homogeneous intrinsic semiconductor unifying parameters of both materials [91],[96]. This principle implies that even if the charge transfer occurs immediately after the exciton generation by the absorption of photons, only bound electron-hole pairs are formed. This suggests a diffusion driven current of these uncharged pairs throughout the bulk. An actual charge separation only takes place at the interfaces to the electrodes. Photovoltaic cells following this principle are therefore expected to be diffusion dominated devices [84], where the *J-V* characteristics should follow a space-charge limited current (SCLC) behavior [108],[145].

3.1.2 Photovoltaic cell performance

Generation of electrical power under illumination is achieved by the capability of the photovoltaic device to produce voltage over an external load and current through the load at the same time. This is characterized by the current-voltage (IV) curve of the cell at certain illumination and temperature (Fig. 3.1). When the cell is

short circuited under illumination, the maximum current, the short circuit current (I_{SC}), is generated. But under open circuit conditions no current can flow and the voltage is at its maximum, called the open circuit voltage (V_{OC}). The point in the IV-curve yielding maximum product of current and voltage is called the maximum power point (MPP).

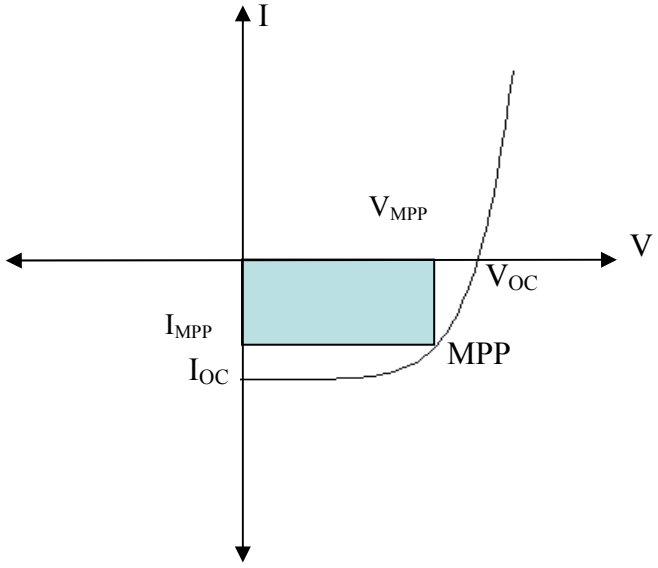

Fig 3.1 Typical shape of the current–voltage curve of a photovoltaic cell showing the open circuit voltage $V_{OC,}$ short circuit current $I_{SC,}$ the maximum power point MPP, and the current and voltage at the MPP; $I_{MPP,}V_{MPP}$

Another important characteristic of the solar cell performance is the fill factor (FF), defined as

$$FF = \frac{V_{MPP} \cdot I_{MPP}}{V_{OC} \cdot I_{SC}} \tag{3.1}$$

Using the fill factor, the maximum power output of the solar cell can be written as

$$P_{MAX} = V_{OC} . I_{SC} . FF \tag{3.2}$$

While the physical principles behind the operation of different types of photovoltaic cells are generally different, the current-voltage curve of well performing cells are similar. Therefor different cells can be characterized and compared with each other in terms of FF, V_{OC}, and I_{SC}. The energy conversion efficiency of the solar cell is defined as the power produced by the cell (P_{MAX}) divided by the power incident on the representative area of the cell:

$$\eta = \frac{P_{MAX}}{P_{light}} \tag{3.3}$$

The efficiency of the solar cell depends on the temperature of the cell and the quality of the illumination. The quality of illumination depends on the total light intensity and the spectral distribution of the intensity. For this reason, a standard measurement condition has been developed to facilitate comparable testing of solar cells between different laboratories. In the standard condition used for testing of terrestrial solar cells, the light intensity is 1000 W/m^2 and the temperature of the cell is 25°C. This intensity value is the integral of the spectral distribution of the light source of AM1.5 (*www.pv.unsw.edu.au/am1.5.html*) global standard solar spectrum (Fig. 3.2).The power output of the solar cell at these conditions is the nominal power of the cell, or module, and is reported in peak Watts, Wp. In practice, special solar

simulator light sources are used for the standard measurements [127].

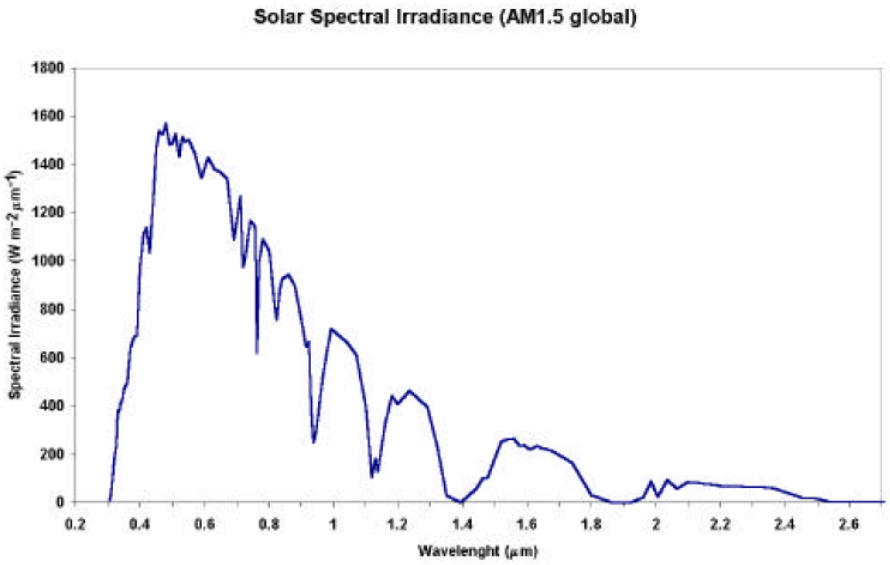

Fig 3.2 The standard AM1.5 global solar spectrum

3.2 Organic Light emitting diodes (OLEDs)

Since the first report of efficient green electroluminescence (EL) from tris (8-hydroxyquinoline) aluminium (Alq3) [242] in 1987 and from poly(p-phenylene vinylene) (PPV) [32] in 1990, tremendous research effort has resulted in a vast literature on organic light-emitting diodes (OLEDs) [26],[32][243]. Reviews of different aspects of the field of OLEDs have appeared, including electroluminescent materials [195] and device physics and engineering [79]. OLEDs have promising application in large area, flexible, full color flat panel electronic displays. Evidence of the considerable progress that has been made in the field is that flat-panel displays based on OLEDs are emerging in commercial products such as cell phones and digital

cameras [248]. Organic light-emitting diodes (OLEDs) possess many advantages including full color capability, potentially low manufacturing costs, high light-emitting efficiency, light weight and wide viewing angle [262].

For the past decade, most attention has been focused on the enhancement of light emitting efficiency, the development of efficient light-emitting materials, and the improvement of device stability 0,[107][242]. OLEDs have evolved into a truly powerful display technology rivaling liquid crystal displays (LCDs). OLED displays are light, durable and efficient and can be built on flexible substrates such as plastics and paper-thin surfaces, creating displays that can be bent or rolled. OLEDs are much more rugged and ideal for portable applications compared to LCDs. Unlike LCDs, OLEDs are self-emitting and require neither backlight, nor chemical shutters that must open and close, making them thinner and more compact.

Light-emitting diodes (LEDs) that incorporate conjugated polymers as the active layer have undergone rapid improvement since the discovery of electroluminescence (EL) from poly(*p*-phenylenevinylene) (PPV) [159]. The 9,9-disubstituted polyfluorenes (PFs) are among the most promising candidates. PFs have been used to demonstrate relatively high photoluminescence (PL) and EL quantum efficiencies and high EL brightness among various polymeric materials [181],[235]. Moreover, as a host material, PFs enable full color via conjugated polymers and with phosphorescent dyes [29],[86],[175].

Despite the ongoing improvements, however, in terms of the stability of polymer LEDs (PLEDs) fabricated from PF-type materials, the lifetime and color

purity need improvement for the commercialization of full-color displays [139][269]. Photo-oxidation plays an important role in the lifetime of PLEDs fabricated from PFs [85]. In addition, most of these PLEDs suffer from a degradation of the device under operation; the degradation is documented in the formation of a low-energy emission band at 2.2–2.3 eV, which turns the desired blue emission color into an undesired blue green emission. These long-wavelength tails become more pronounced upon exposure to heat (for example, the Joule heat generated during the operation of LEDs) [134],[181].

One of the key challenges on the path to developing the next generation of high-performance OLEDs is the design and synthesis of readily processable and thermally robust emissive and charge transport materials with improved multifunctional properties. OLEDs are double charge injection devices, requiring the simultaneous supply of both electrons and holes to the electroluminescent (EL) material sandwiched between two electrodes. To achieve an efficient OLED with the single-layer configuration, the organic EL material would ideally have a high luminescence quantum yield and be able to facilitate injection and transport of electrons and holes. This demand of multifunctional capabilities from a single organic material is a very difficult one to meet by nearly all current materials. Most highly fluorescent or phosphorescent organic materials of interest in OLEDs tend to have either p-type (hole-transport) or n-type (electron transport) charge transport characteristics [26],[32],[242],[243]. A consequence of this is that the simplest OLED configuration, where an organic emitter layer is sandwiched between a transparent

anode and a metallic cathode, gives very poor efficiency and brightness [26],[32][79],[195],[243]. The use of two or more different materials to perform the required functions of efficient light emission and good electron- and hole-injection and transport properties in an OLED has resulted in orders of magnitude improvement in device performance [26],[32][79],[195],[243].

3.3 Organic field effect transistors (OFETs)

Organic field effect transistors based on organic molecules, or conjugated polymers, have attracted considerable attention because of attributes that complement silicon-based large-scale integration devices that are high-performance but expensive. Organic transistors can be manufactured on plastic films at low (ambient) temperatures; therefore, they are mechanically flexible. The processing characteristics and demonstrated performance of OFETs suggest that they can be competitive for novel thin-film transistor applications that require large-area coverage, structural flexibility, low-temperature processing, and low cost.

3.3.1 Current research progress in OFETs

Currently, OTFTs have already shown promising applications in electronic papers [82],[199],[216], circuits for active-matrix OLED displays [82],[199], sensors [45],[224],[225][270], and radio frequency identification cards (RFIDs) [13],[252].

The key parameters characterizing a FET include the field-effect mobility (μ) which quantifies the average charge carrier drift velocity per unit electric field and the on/off ratio (I_{ON}/I_{OFF}) defined as the drain-source current ratio between the “on” and

"off" states. For a high-performance OFET, μ and I_{ON}/I_{OFF} should both be as high as possible. For most practical applications, the mobility of the field-induced charges must be greater than 0.1 $cm^2/(V\ s)$. Another issue in research into organic thin-film transistors (OTFTs) is low-voltage operation. Current research results show that transistors based on polycrystalline films of pentacene set the benchmark for OTFT performance. A device with excellent electrical characteristics such as field-effect mobility of 1.1 cm^2 /V s, a threshold voltage of −0.98 V, and I_{ON}/I_{OFF} of 10^8, has been reported [113],[168],[220].

To enable low-cost OTFT circuits, it is critical that useful transistor functionality be achieved under ambient fabrication conditions and that the OTFTs possess the required stability for long-term operation. However, not many organic semiconductors have both the mobility and stability to enable these practical applications. Three primary classes of p-channel organic semiconductors are: (1) acenes such as tetracene, pentacene, and their derivatives [93], (2) oligothiophenes and polythiophenes [219], and (3) fused-ring thiophene-aromatics [133] and thiophene-vinylene/arylene derivatives [251] Most of these semiconductors have relatively high-lying HOMOs and narrow bandgaps. They are therefore easily photooxidized, resulting in degraded semiconductor characteristics when processed in air or operated in ambient conditions. Very recently, certain oligofluorene derivatives have been reported to have high FET mobility and good stability [267]. One of the most important stability issues in organic transistors is the shift in the threshold voltage upon applying a bias to the gate electrode. This is called stressing. The

applied negative gate potential for a *p*-type semiconductor causes a buildup of mobile charges at the semiconductor/insulator interface, which are then trapped. As a consequence, to reach an identical channel current subsequently, a higher gate voltage has then to be used. Bias stress effects have been reported for transistors based on pentacene, polythienylene vinylene [28],[152],[271], α-sexithiophene [202], poly-9,9-dioctyl-fluorene-cobithiophene, and regioregular-polythiophene [202],[231]. Several authors have also reported that the threshold voltage shift is reversible, and that the recovery process can be enhanced by a positive gate bias [209],[231]

In addition to stability, the high contact resistance present at the interface between the metal electrodes and the organic semiconductor [31] is a great concern of organic field-effect transistors (FETs) at present. In spite of the large effort put in the investigation of contact effects [31],[155],[167],[182],[215],[230], the reason for both the high values and the irreproducibility of the contact resistance are not currently understood. It might be the collective effect of different phenomena, including the presence of grain boundaries at the metal/organic interfaces, fluctuations in the work function of the metal electrodes, and others.

3.3.2 Basic structure of OFET

An organic thin film transistor is composed of three basic elements: a thin semiconductor film, an insulating layer, and three electrodes. Two of them, the source and the drain, are in contact with the semiconductor film at a short distance from one another. The third electrode, the gate, is separated from the semiconductor film by the

insulating layer. Its structure is similar to that of a traditional silicon metal-oxide-semiconductor field effect transistor (MOSFET). Fig. 3.3 shows the structures of common top contact and bottom contact OFETs.

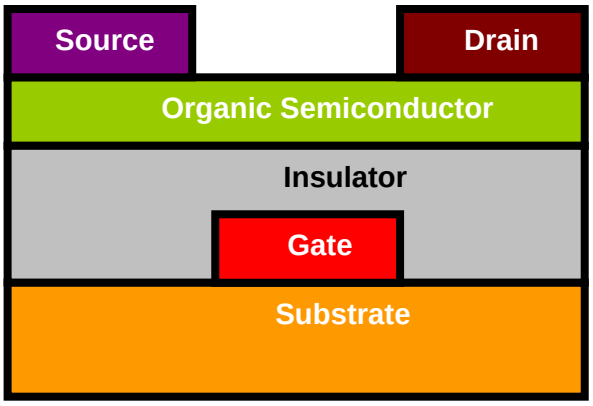

(a) Top contact

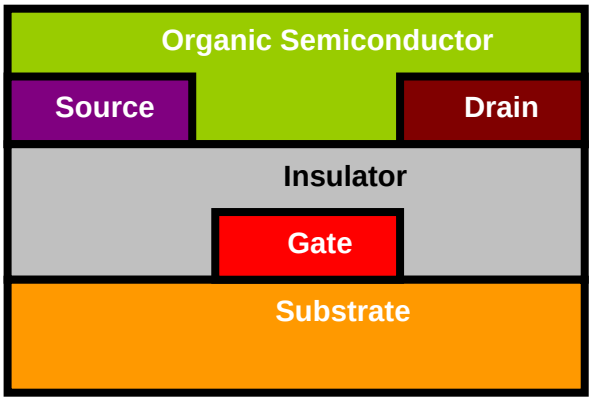

(b) Bottom contact

Fig 3.3 Typical device structures of OTFTs: (a) top-contact and (b) bottom-contact. [140]

The structures are inverted in the sense that the channel and the source/drain are on top of the gate, in contrast to silicon MOSFETs. The heavily doped silicon

serves as the gate electrode. Silicon dioxide is the insulator, polymer is the channel layer, and gold is the source/drain electrode. These transistors are also called thin-film-transistors, because structurally, the channel material is a vacuum-deposited thin film (about 100 nm). The metal source and drain electrodes are often vapor-deposited through a shadow mask, but conductive inks that can be printed are also employed. Source-drain channel lengths, L, typically range from 10 to 100 μm, and channel widths, W, are usually between 100 μm and 1 mm [170]. These transistors are field effect transistors; they operate by changing the conductance of the channel by modulating the charge with the gate field.

In a traditional inorganic device, the active semiconductor layer is generally comprised of lightly doped Si. In these materials, the applied gate voltage causes an accumulation of minority charge carriers at the dielectric interface, e.g. electrons in a p-type material, termed an inversion layer. In this very shallow channel, carriers injected from the source and drain electrodes may pass, resulting in current flow. In an organic transistor, the active layer is comprised of a thin film of highly conjugated small molecules or polymers. In contrast to inorganic materials, organics pass current by majority carriers, and an inversion regime does not exist. This fundamental difference is related to the nature of charge transport in each of these semiconductors. Most of these organic semiconductors are *p*-channel materials [54],[81],[106],[252] and only a small fraction are found to function as *n*-channel semiconductors]. [9],[44],[117].

4. SPECTROSCOPIC STUDY

Enhancing the electrical and optical properties of a material using a composite formation has been widely practiced in both academia and industry. In this chapter and in the next two chapters we present our experimental results from a variety of organic composites. These nanocomposites are studied spectroscopically before being tested for device application. The spectroscopic studies give information about the charge transfer and interaction between the different components of the composite.

4.1 C_{60}–poly(*m*-phenylenevinylene-co-2,5-dioctoxy-p-phenylenevinylene) nanocomposite

Developing new materials for optoelectronic applications can be done by forming composites that utilize the properties of two materials to provide an enhanced composite system [37],[38],[48]. Recently, nanocomposites made of donor and acceptor materials have attracted the attention of the scientific community for applications in solar cells [196],[257],[268]. Promising results for improving the efficiency have been reported for solar cells made of polymer/C_{60} blends [185],[196],[257],[268]. In such blended structures, the excited states are dissociated at the polymer/ C_{60} interface and the recombination process is inhibited by the spatial separation of the charged particles [3]. This improves the efficiency of the sandwich cell. Organic diodes made from conjugated polymer/ C_{60} heterojunctions have shown a high rectification ratio [203].

However, the application of C_{60} for these suggested areas is limited by its

poor solubility in most organic solvents and the difficulty to control its aggregation tendency [165]. To avoid this problem considerable effort has been done and successful results have been reported which show an increase in the solubility of C_{60} by means of attachment of C_{60} to water soluble polymers [115],[227],[266] and chemical modification of fullerenes [33],[78],[179],[245].

Previous work on carbon nanotube composites has shown that the helical nature of poly(*m*-phenylenevinylene-co-2,5-dioctoxy-p-phenylenevinylene) (PmPV) with an added dihedral angle allows it to overcome steric barriers [48]. It helps the polymer to wrap itself around the tubes and maintain a regular crystallized structure more easily [153]. This attachment plays a major role in its ability to bind by means of π–π interactions. It also helps to increase conductivity, which can be observed via a percolation process [47]. Based on this information, we anticipate that PmPV (the structure is shown in Fig. 4.1) will wrap the C_{60} balls up in the helix and increase the fullerenes' solubility while also reducing the fullerenes' tendency to aggregate.

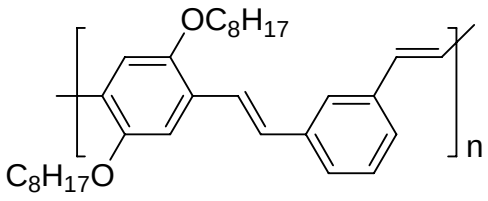

Fig 4.1 Repeat monomer unit of poly(m-phenylenevinylene-co-2,5-dioctoxy-p-phenylenevinylene) (PmPV).

PmPV is a substitute form of poly(p-phenylene vinylene) and is characterized in the absorption spectra with a strong broad absorption feature near 420 nm [229]. Polymer-fullerene nanocomposites are usually made either by a direct blending of the polymer with the fullerene or forming a supermolecular system by attaching a properly functionalized fullerene to the polymer backbone [112],[68]. The photo generation efficiency of the device made from this composite depends on the spectral absorption and on the availability of an efficient transport path for the generated free charge carriers toward the electrodes [41],[169]. It has been recommended that the covalently linking of donor acceptor systems would be an efficient mechanism for the production of ambipolar "double cable" transport channels [41],[42]. This mechanism also removes the question of compatibility between the conjugated polymer and fullerene components. Phase separation and clustering of C_{60} in the blend structure can reduce the energy conversion efficiency of the composite [41]. In addition, as the fullerene molecules have low light absorbance in the visible range [244] the composite made from the mixing of fullerene and polymer can suffer from low light absorption.

We prepare solutions of PmPV in toluene with a concentration of 20 g/l. This solution is doped with C_{60} at loadings of 2.5%, 5%, 7.5% and 10% in weight. Then the composite is sonicated for two hours to get a well dispersed composite. UV-Vis absorption spectroscopy is done in a solution form using a Perkin Elmer Lambda 20 UV-Vis spectrometer with a 1 cm path length quartz cell.

Analyzing samples with near field optical microscopy enables us to overcome

the lateral resolution limit of the classical optical microscopes imposed by far field diffraction phenomena [2]. In Near field Scanning Optical Microscopy (NSOM) (in this case Veeco's Aurora 3), the laser (457 nm) is guided to an aperture via a straight optical fiber. The aperture is tapered to a diameter of approximately 100 nm and coated with a metal, such as Al. The tip was placed in close proximity to the composite surface (near field region ≈ 10 nm) and the interaction between laser light passing through the aperture and the sample was limited to the aperture diameter [17],[43]. The NSOM instrument is a combination of a scanning probe microscope, which probes the topographic image, and an ultra high resolution optical microscope. Used as an optical microscope, the NSOM can be operated either in transmission, reflection or lithographic modes. The major techniques of the transmission mode are bright field, fluorescence, polarization, and spectroscopy. A tuning fork-based shear force feedback mechanism and an optical feedback mechanism are the main control techniques to control the distance between the probe tip and the sample. In our case the near field optical microscopy was carried out on thin films of the composite spun onto a glass substrate.

Thin films of the sample were prepared by drop casting onto a silicon substrate for resonance Raman spectroscopy. The Raman spectra for 785 nm and 514 nm laser lines were taken using a Renishaw InVia Raman spectrometer equipped with a Raman Leica RE02 microscope.

4.1.1 UV-Visible Spectrometry

Fig. 4.2 shows the optical absorption spectra for pure PmPV and PmPV/C_{60} composite with several concentrations of C_{60}. The PmPV spectrum shows the onset of the spectrum at about 2.45 eV, which is due to the π-π* transition of the PmPV backbone, and two other broad peaks at 3.5 eV and 4.19 eV. Absorption spectra of the PmPV/ C_{60} composite indicate that the characteristic C_{60} absorption peak at 3.7 eV [204] was washed out by the PmPV absorption. The peaks of the composite below the π-π* gap of the host polymer evolve with increasing concentration of C_{60}. Those are the peaks at 2.32 eV and 2.09 eV. The peak at 2.32 eV is the onset of photocarrier generation [118]. The onset of the peak at 2.09 eV is about 1.8 eV which is slightly less than the threshold of the band between the highest occupied molecular orbital and the lowest unoccupied molecular orbital, which is 2.1 - 2.3 eV for C_{60} [141][218],[239].

As suggested earlier in this chapter, the C_{60} buckeyballs might be encapsulated in the helix of PmPV and this can result in electronic confinement. This confinement has been observed when an antracene is incorporated in Zeolites pores [149]. It has been predicted that this phenomenon results from a reduction in the bandgap of the guest molecule relative to its normal state. The longest wavelength absorption peak of C_{60} around 2 eV, which is supposed to correspond to the singlet energy [4],[194], appears only as a small shoulder in our work. Generally, the presence of C_{60} did not affect the peaks of PmPV. Similar effects have been reported for a composite made from poly(2-methoxy,5-(2'ethyl-hexyloxy)-*p*-phenylene

vinylene) and C_{60} [221]. When the distance between donor and acceptor is short, their interaction can be seen from the ground state absorption [124]. This interaction can be observed by the appearance of new peaks in the near infrared or by the shift of the absorption peaks of the composite relative to the pure component materials [80].

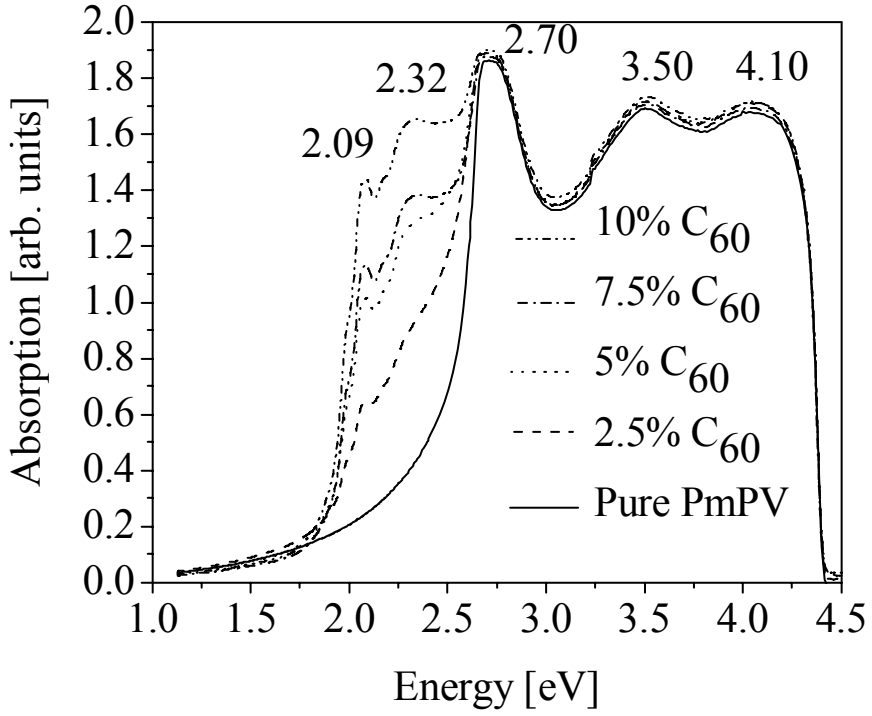

Fig 4.2 UV-Visible spectra PmPV/C_{60} nanocomposite for different concentrations of C_{60}.

4.1.2 Fluorescence Spectra and Atomic Force Microscopy

We have also characterised our sample with fluorescence near-field spectroscopy and atomic force microscopy. Fig. 4.3 shows the topographic image of PmPV/C_{60}. The white spots are clusters of C_{60} in the PmPV matrix. Previous

photoluminescence studies show the coupling of C_{60} molecules in the excited dimer [188],[249]. Fig. 4.4 shows the corresponding fluorescence spectra for (a) PmPV and (b) PmPV/ C_{60} composite (b). The major fluorescence peak of PmPV around 500 nm [259] appears at about 487 nm. The composite sample has shown a fluorescence peak which is red shifted by about 10 nm relative to the pure PmPV spectrum. The minor peaks at a wavelength close to the excitation wavelength are probably the direct reflections of the excitation laser.

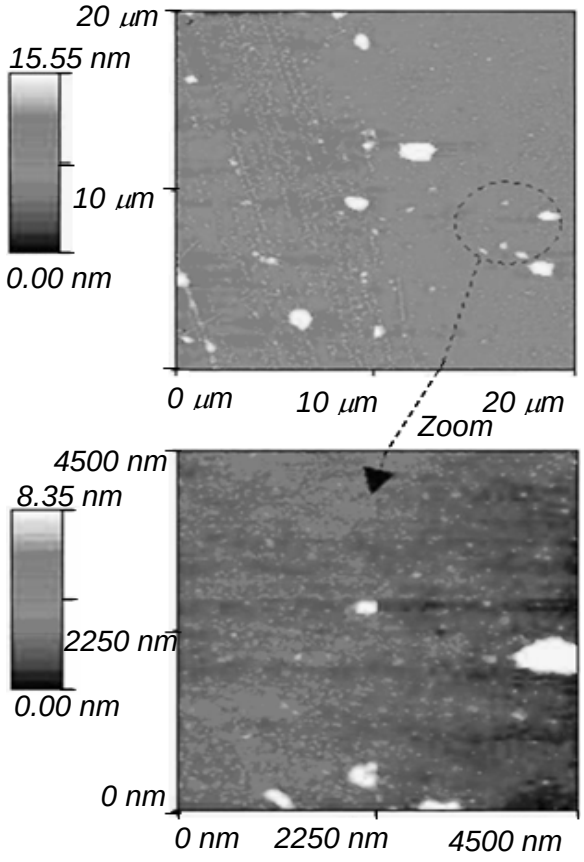

Fig 4.3 Atomic Force Microscopy topographic images of PmPV/C_{60} nanocomposite.

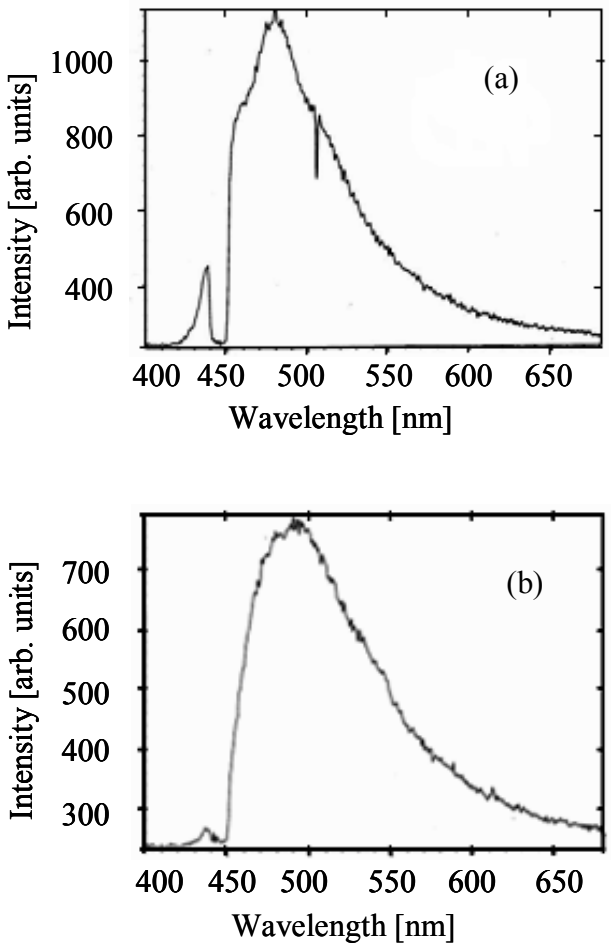

.

Fig 4.4 Near field fluorescence spectra of PmPV (a) and PmPV- C_{60} composite (b)

4.1.3 Raman Spectroscopy

The Raman spectra for the pure PmPV and PmPV/C_{60} composite were taken using 785 nm and 514 nm laser lines. Fig. 4.5(a) shows the spectrum for the 785 line with bottom spectrum for pure PmPV. The major peaks of PmPV are 1577 cm^{-1},

corresponding to the C-C stretching of the phenyl ring [123], 1600 cm^{-1}, corresponding to the vibration "quadrant stretch" mode of the di-substituted benzene ring component of the monomer [123], and 1629 cm^{-1} corresponding to the C=C stretching mode of the vinyl group on the polymer back bone. These peaks, in general, are unaffected by the incorporation of C_{60} [122],[155].

The Raman spectra of the composite show two notable differences from the spectrum of the pristine polymer. These are the broadening of the already existing peak at 624 cm^{-1} and the new broad peak appearing around 1850 cm^{-1}. This difference is due to the excitonic effects formed by the transfer of electrons from the conjugated polymer to fullerene. It is a well understood phenomenon that occurs when self localized charged states are formed in a polymer backbone, as a result of doping or photoexcitation [63],[157]. The intensity of the new broad peak at 1850 cm^{-1} depends on the concentration of C_{60} and is in resonance to the 514 laser line Fig. 4.5 (b). The electron transfer between the donor and acceptor materials might induce vibration, which in turn induces a change in the polarizibility of the composite. The overall effect could be the broadening of the Raman peaks or initiation of new Raman active modes [138],[255]

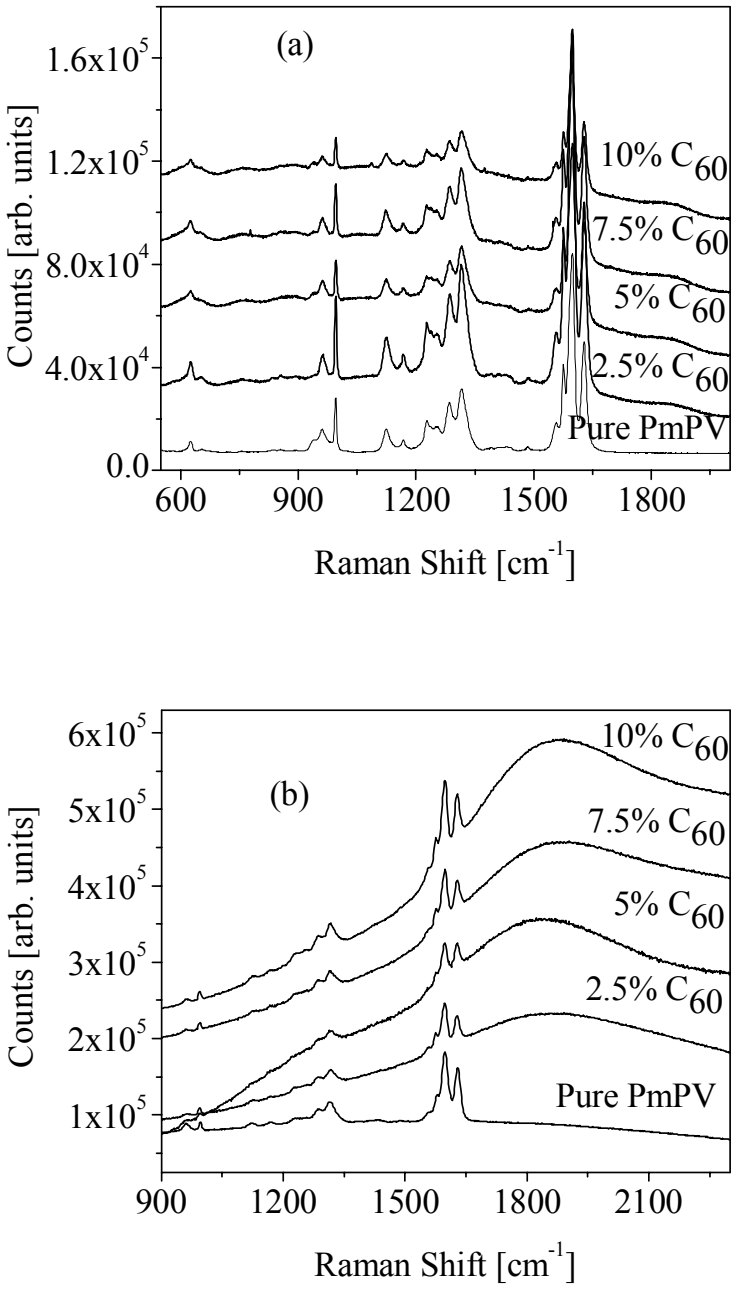

Fig 4.5 Raman Spectra of PmPV/C_{60} composite for 785 (a) and 514 (b) laser lines.

4.2 Polymer, Single Wall Nanotube, and Dye Composite.

Improving the efficiency of organic solar cells relies on improving the transport and light absorbance properties of the materials being used. Improving the charge separation and charge transport by forming composites of polymer and fullerenes is addressed in Section 4.1. Here we present a work on a composite which tries to address both transport and absorption. This composite is made from Polythiophene 506, SWNT and Eosin.

Organic semiconductors have typical opticalband gaps around 2.0 eV, which is considerably higher than that of crystalline silicon. This high band gap results in a spectral mismatch between the absorbance of the organic material and the white light spectrum. The optical bandgap of PPV and polythiophene derivatives that are currently used in the applications of polymer-fullerene solar cells are in the range between 2.2 and 1.9 eV. This bandgap is also not optimal with respect to the solar spectrum. One strategy to avoid this problem is to use materials with enhanced light absorption properties. This can be achieved by applying a low bandgap material with an optical band gap below 1.8 eV. The promising candidates for this strategy are dyes, which have a high absorption coefficient.

We analyzed the composite using UV-Vis absorption and fluorescence spectroscopy. The transport property and device application of this composite is given in chapters 5 and 6.

4.2.1 UV-Vis Absorption

Fig. 4.6 (a) shows the absorption spectra of Eosin dye and Eosin attached SWNT. A slight blue shift of the major peak at 540 to 537 nm and a new broad peak appears at 393 nm. The absorption spectra of the composite is presented in Fig. 4.6 (b). The spectrum consisting of a peak at 540 nm and a less intense shoulder on the short-wavelength side is the typical absorption spectrum of Eosin.

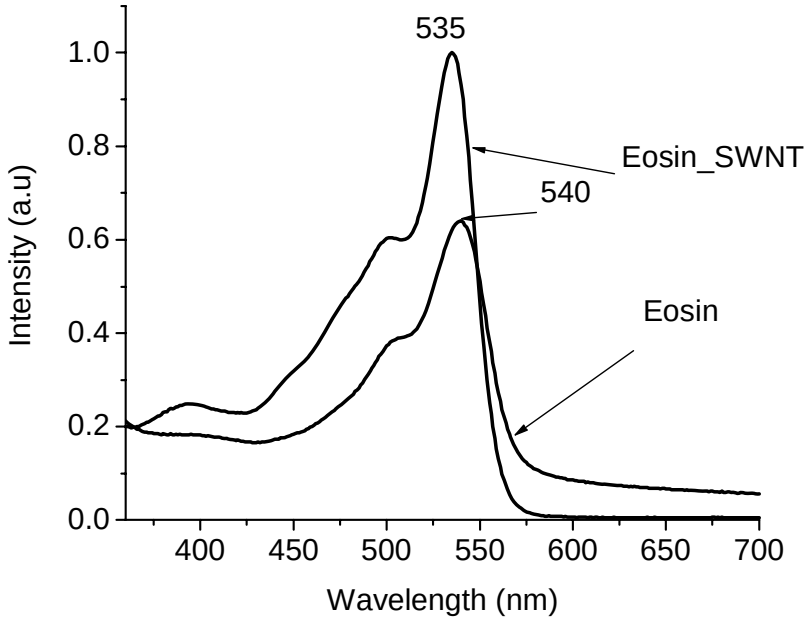

(a)

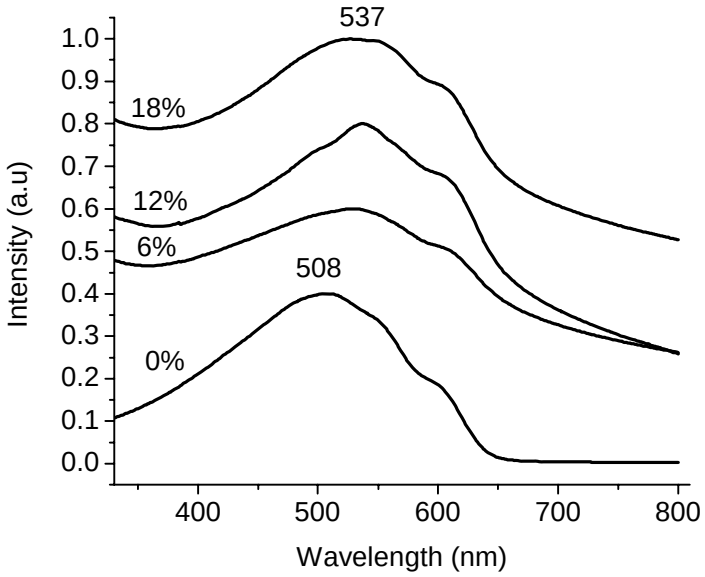

(b)

Fig 4.6 UV-Vis Absorption spectra of (a) Eosin dye and Eosin attached SWNT and (b) different concentration of Eosin_SWNT in Polythiophene 506

Comparing the pure polymer spectrum with the spectra of the composite shows the peak at 508 for the pure polymer is red shifted by about 29 wavenumbers. But the shoulder at 600 nm doesn't show significant shift. No major difference is observed between the spectra for different concentrations Eosin_SWNT in Polythiophene 506.

The composite made from these three materials shows both shifting and broadening of the peak at 508nm to 537nm. The large broadening of the composite absorption spans the visible spetrum from 400 to 700 nm. This broadening of spectrum in the visible compared to the spectra of the individual materials shows the

composite is a better material in increasing the absorption efficiency of devices. It is obvious that the strong electrostatic interaction and charge sharing between the dye, polymer, and SWNT is responsible for these absorption changes.

4.2.2 Fluorescence

The fluorescence spectra of the composite, in solution form, is investigated with Varian Carry Spectrometer with a mirocell of size 400 µl.

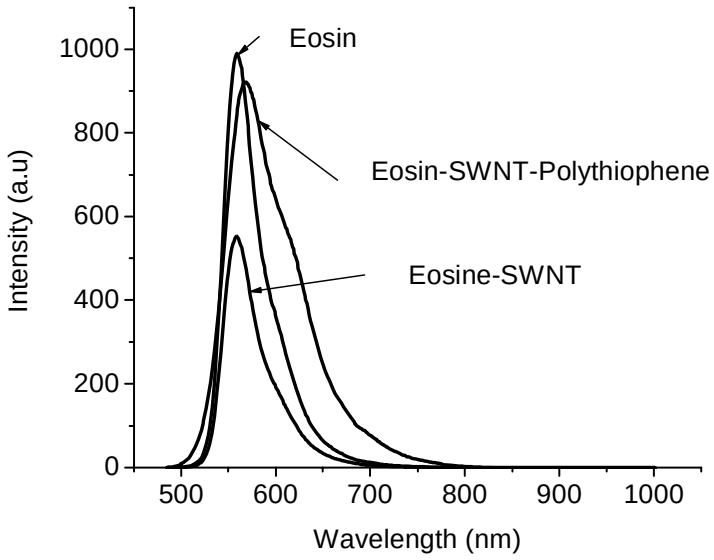

Fig 4.7 Fluorescence spectra of Eosin dye, Eosin_SWNT, and Eosin_SWNT_Polythiophene 506

Fig. 4.7 presents the spectrum of Eosin, Eosin/SWNT, and Eosin/SWNT/polymer composite. The intensity peaks of Eosin and Eosin/SWNT are at 559 nm whereas the composite with the polymer shows a peak at 569 nm, which is

red-shifted by about 10 nm from Eosin spectrum.

Both absorption and fluorescence spectroscopy shows shifts of the composite spectra relative to the spectrum of the individual component materials. This indicates the presence of electronic interaction both in the ground and excited states. This interaction leads to the formation of polarons.

The main objective of the spectroscopic study of the composites given in this chapter was to check whether we have been able to get an electrical interaction between the component materials and able to create charge carriers in the composite matrix. All the spectroscopic results on PmPV-C_{60} composite confirmed the existence of charge transfer between PmPV and C_{60}. The UV-vis and fluorescence study of Polymer, SWNT, and dye composite have shown both a shift and broadening of a spectrum. Based on these spectroscopic results, we have performed transport studies on the composites and made devices on Polymer, SWNT, and dye composite. The results are given in chapters 5 and 6.

5. ELECTRICAL TRANSPORT

Two point probe conductivity measurements are carried out on drop cast films of the nanocomposites on vacuum deposited gold electrodes on glass. The deposition is done using a vacuum depositor at about 6.7×10^{-4} Pa. Contacts across the electrodes are made using gold wire and conductive silver paint as shown in Fig. 5.1.

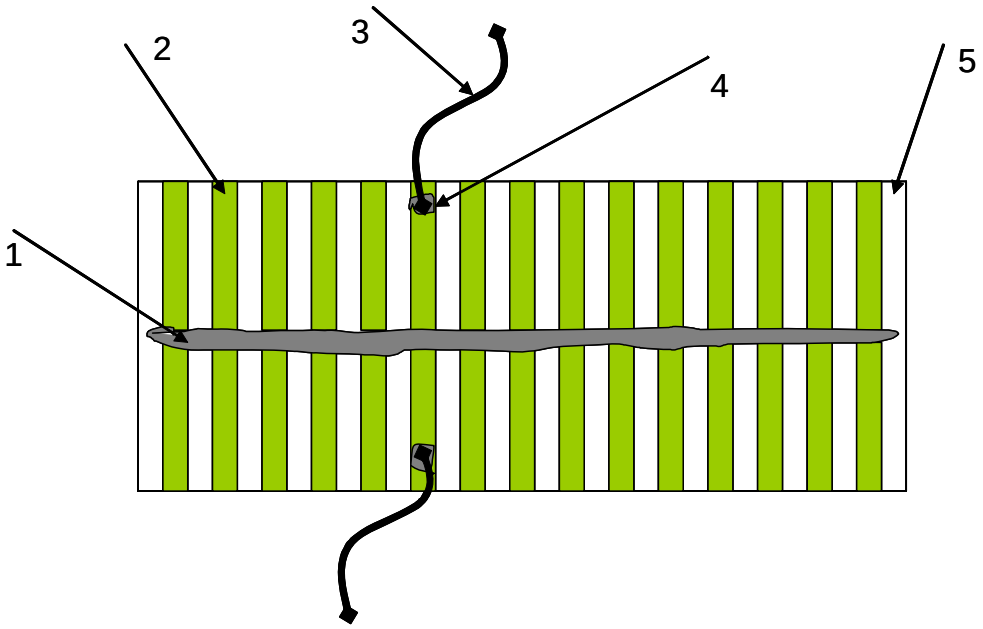

Fig 5.1 shows a typical conductivity measurement sample prepared on a glass substrate.

1. dropcasted thin film of composite (polymer) for characterization
2. vacuum deposited gold thin film
3. gold contact wire
4. silver paste
5. glass substrate

5.1 C_{60}–poly(*m*-phenylenevinylene-co-2,5-dioctoxy-p-phenylenevinylene) nanocomposite

We carry out conductivity measurement to investigate the effects of C_{60} on the conductivity of the polymer due to a donor/acceptor effect. Conductivity measurements are made using a Keithley 6487 Picoammeter/voltage supply instrument.

Fig. 5.2 shows both the dark and photo conductivity of the composite for different concentrations of C_{60}. As can be seen from the graph, the conductivity shows a slight concentration dependent increase for both dark and photo conductivities

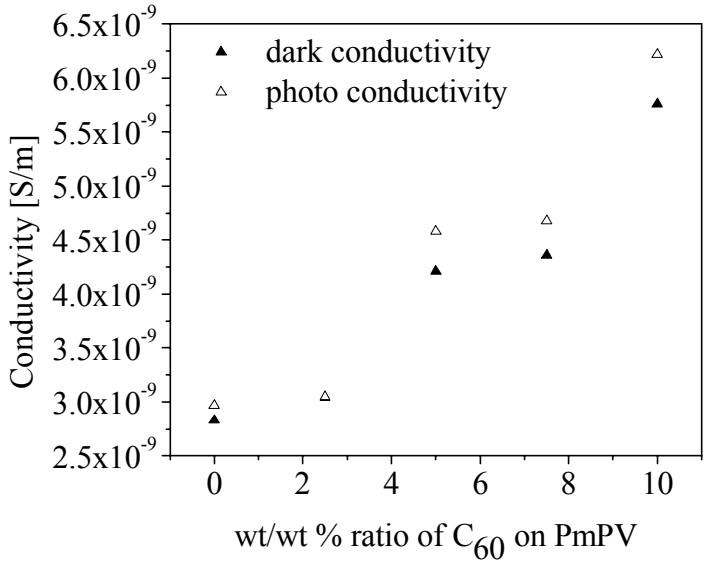

Fig 5.2 Dark and photo conductivity of polymer/C_{60} composite for different concentrations of C_{60}

In going from 0 to 10% loading, the conductivity for both dark and photo

conductivities increases by a factor of about 2. This increase is characteristic of an excited state exciton generation, where the PmPV acts as a hole carrier and the C_{60} acts as an electron carrier [136]. A high increase of photoconductivity, when π-conjugated polymers are doped with C_{60}, has been reported previously [52]. Composites made of polymers such as poly(p-phenylene vinylene), poly(3-alkylthiophene), poly(octylthiophene) and C_{60} [137],[204],[221] have also shown a similar increase in photoconductivity.

However, in our case we didn't see a significant increase in conductivity by the presence of C_{60}. As evidenced by the NSOM topographic imaging, the structure and morphology of the composite not being perfectly blended at the nanoscale, may have a negative effect on the free charge carrier formation by preventing the overlap of the donor acceptor excited state wave functions [22],[214]

Both dark and photoconductivity results show a slight increase in conductivity which depends on the concentration of C_{60}. This implies that there is an electron transfer from the conjugated polymer PmPV to C_{60}. This is confirmed by all the spectroscopic experiments - absorption, fluorescence, and Raman spectroscopies. Since this increase in conductivity is small compared to the results obtained from the studies of some other polymer/C_{60} composites, we conclude that morphological effects could possibly account for this decrease in the electron transfer process. We also see an increased generation of excitons which are responsible for many of the electronic properties found in the most common and efficient polymer-based electronic devices. The existence of excitons in conjugated polymers makes the

polymer a candidate for optoelectronic applications. Since the composite shows an increase in conductivity, it could be anticipated that the controlled chemical doping of PmPV with fullerene might give a significantly enhanced conductivity for possible solar cell applications.

5.2 Polymer-multi wall carbon nanotube composites

Since their discovery in 1991, nanotubes, whether they appear in the form of multi-walled or single-walled versions, have attracted much research interest [62],[111]. It is thaught that carbon nanotubes possess unique combination of properties, such as high-mechanical strength [247], high electrical and thermal conductivity, as well as high-thermal stability [103],[214]. A wide range of possible technological applications, which include nanoelectronics [76], field emission guns [50], and ultra strong materials [18], have been foreseen. It is now widely accepted that electrical and thermal management in nanosize devices has become increasingly important as the size of devices has been reduced [51],[256]. Therefore, the thermal and electrical conduction of nanometer materials plays a fundamentally critical role that controls the performance and stability of nano/micro devices. When combined with conjugated or non-conjugated polymers, these novel materials possess potentially fascinating applications as electronic devices or re-enforced nanocomposite materials [105],[171]. Among various potential materials that will be used in Micro Electro Mechanical Systems (MEMS), Nano Electro Mechanical

Systems (NEMS), and "smart structural materials" for aerospace, carbon nanotube nanocomposites stand in a unique position [49],[144].

We prepare a composite from polystyrene and multi-walled carbon nanotubes (MWCNT) and investigate the electrical transport properties of the composites. From this dynamic electrical transport study, enhancement of charge transport through covalent bonding is seen.

Unlike traditional techniques of composite formation, we choose to polymerize styrene from the surface of dithiocarboxylic ester-functionalized MWCNTs to fabricate a unique composite material, a new technique dubbed "gRAFT" polymerization.

Thin films of the nanocomposite are spin-cast from a THF solution. At lower MWCNT loadings (< 0.9 wt %) a 500 μm thick film is optically transparent and we do not observe any aggregation of the nanotubes in the film visually. Nanocomposite conductivity, as a function of dithioester MWCNT loadings, is measured on the spin-cast thin film by a two point probe method using vacuum deposited gold as electrodes. The plot of $\log_{10}$(conductivity) vs MWCNT wt % (0.02 – 0.9 wt %) shows two distinct transport regions associated with nanotube loadings and corresponding polymerization (Fig. 5.3 inset). These regions suggest two different charge transport mechanisms: charge hopping in low MWCNT loadings (0.02-0.6 wt %) and ballistic quantum conduction in high loadings (0.6-0.9 wt %). The composite exhibits dramatically enhanced conductivity up to 33 S/m at a MWCNT loading of 0.9 wt %.

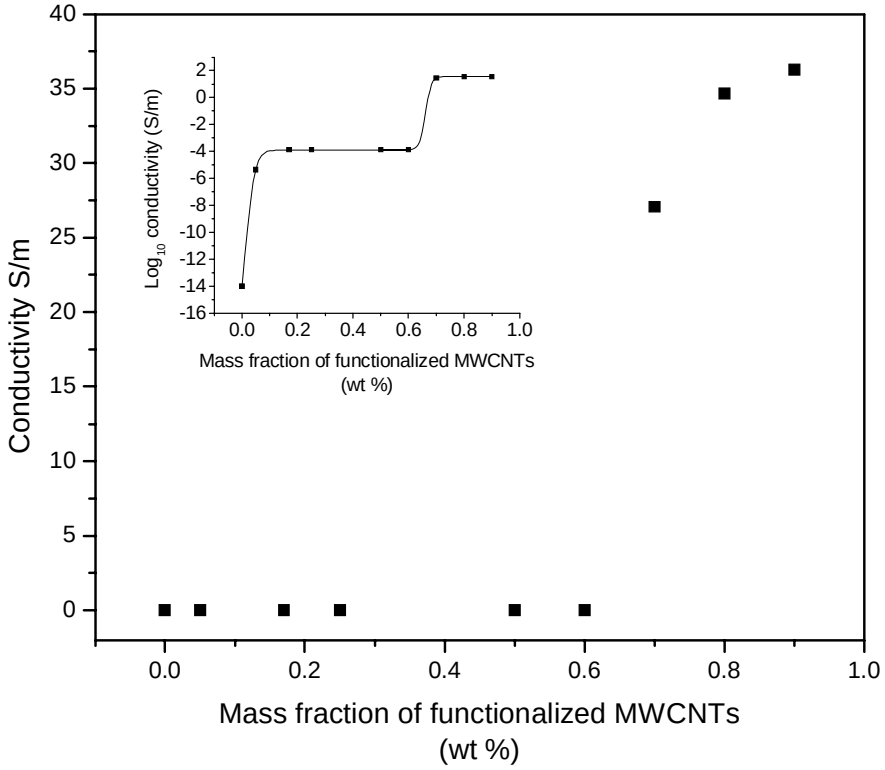

Fig 5.3 A plot of DC conductivity of covalently linked MWCNT-polystyrene composite as a function of mass fraction of functionalized MWCNTs in the composite. Inset: a semilogarithmic plot of covalently linked MWCNT-polystyrene composite conductivity as a function of mass fraction of MWCNT in the composite.

Previously, in studying the percolation network of polypyrrole in conducting polymer composite, Fourier *et al.* analyzed the insulator-to-conductor transition according to percolation theory. They proposed an analytical model [74] to fit the experimental data of composite conductivity:

$$\log_{10}(\sigma_c) = \log_{10}(\sigma_n) + \frac{\log_{10}(\sigma_p) - \log_{10}(\sigma_n)}{1 + e^{[b(p-p_c)]}} \tag{5.1}$$

where σ_c, σ_n and σ_p are the conductivities of the composite, nanotubes and pristine polymers respectively, p is the mass fraction of the nanotubes, and b is an empirical parameter that leads to the change in conductivity at the percolation threshold (or ballistic threshold) p_c. Equation (5.1) has been fitted to profile (1) and (2) individually (Fig. 5.3 inset). Profile (1) gives a percolation threshold (p_{c1} = 0.014 wt %) for lower MWCNT loadings, due to the homogeneity of the MWCNTs in the polystyrene matrix. This indicates the formation of a conducting pathway in the composite, which allows charge transfer through a hopping transport regime. This pathway results in an increase in conductivity from 10^{-14} S·m^{-1} for pure polystyrene to 10^{-4} s·m^{-1} at MWCNT loadings of 0.02-0.60 wt %.

In profile (2) we see a second percolation threshold (p_{c2} = 0.66 wt %) with conductivities between 10^{-4}– 33 S·m^{-1} for nanotube loadings 0.60–0.90 wt % (Fig. 5.3). The solid line in Fig. 5.3 represents two curve fits using (5.1). For profile (1) the parameters for best fit are: 0.02 wt % ≤ p < 0.6 wt %; p_{c1} = 0.014 wt %; b = 63; and for profile (2) 0.6 wt % ≤ p ≤ 0.9 wt %; p_{c2} = 0.66 wt %; b = 96.

In the past, a percolative description has been used to explain the connectivity of conductivity of a random two-phase system when examining nanotube-polymer composites [37]. In certain cases, where MWCNTs are added to an insulating polymer to form a blend, the onset of percolation is found to be more than 1% by weight [156],[190].

To have a comparison between the charge transport properties of the composites made using the gRAFT method and the usual blend formation method,

we have blended MWCNT and polystyrene and measured the electrical property of the composite. For our blend containing polystyrene and pristine MWCNT (0-20 wt %) without thiolation, a single-stage percolation was observed with a percolation threshold at 4.7 wt % MWCNT loading and the maximum conductivity of 2.0×10^{-4} $S \cdot m^{-1}$ at 12 wt % or higher pristine MWCNT loading (Fig. 5.4 and inset).

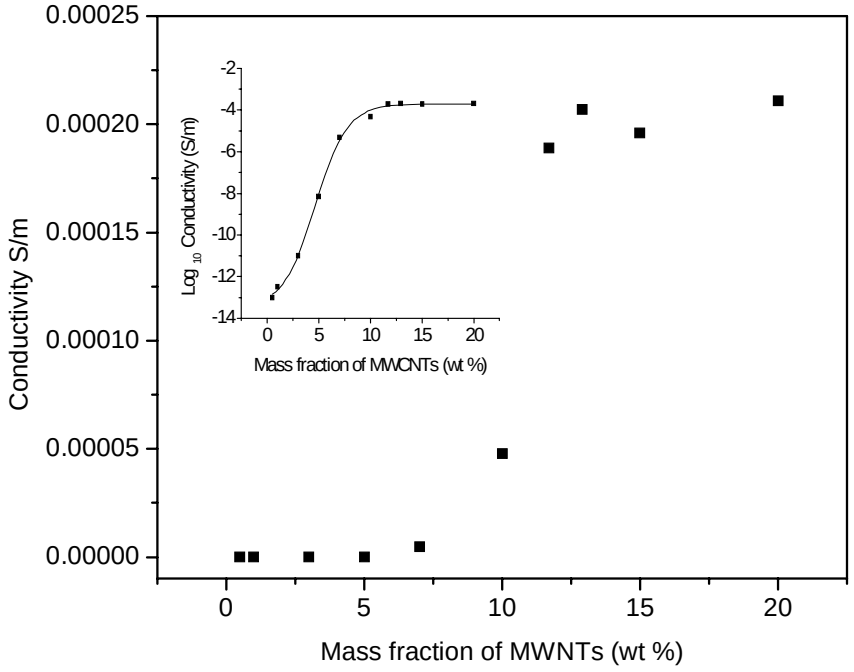

Fig 5.4 A plot of DC conductivity of pristine MWCNT-polystyrene blend as a function of mass fraction of pristine MWCNTs in the blend. Inset: a semilogarithmic plot of pristine MWCNT-polystyrene blend conductivity as a function of mass fraction of pristine MWCNT in the blend. The solid line represents a curve fit using (5.1)

The percolation threshold in this case is significantly higher than what was observed in our covalently linked MWCNT-polystyrene composite prepared through *in situ* gRAFT polymerization. The maximum conductivity for the blend is much

lower than the covalently linked MWCNT-polystyrene composite.This increase in conductivity further indicates the significance of good nanotube dispersion for high conductivity and the effectiveness of our synthetic method.

According to recent reports, theoretical calculations have shown that the onset of percolation of conductivity was strongly dependent on the aspect ratio defined by $a = l/d$ where d is the diameter, l the length, and a the aspect ratio [75]. Foygel *et al* suggest that conductivity would be changed and increased with altering aspect ratio in a three dimensional system. This would suggest that the strength of conductivity we have observed as well as the low value of onset of percolation can be directly related to the changing dimensions of the nanotubes present.

5.3 PmPV-Gold nanocomposite

In this work we have embedded micron-sized gold nanoclusters into a conjugated luminescent polymer poly(*m*-phenylenevinylene-*co*-2,5-dioctoxy-*p*-phenylene) (PmPV) thin film matrix, thus creating a unique nanocomposite. This embedding of micron-sized gold nanoclusters into a PmPV thin film matrix is achieved by utilizing the helical binding properties of PmPV. The gold clusters are composed of approximately 5-50 nm PmPV passivated gold particles.

We have studied the eletrical transport property of the composite and the Schottky effect of the sandwich cell device made out of it. The dc conductivity studies are undertaken to investigate the effects on conductivity due to the presence of nanoscale metallic particles in the polymer matrix. By doping the polymer with gold

we observe only a slight increase in conductivity at loadings of ~30% wt/wt gold to PmPV. The incorporation of gold into the PmPV matrix results in only a slight increase in conductivity. We observe typical ohmic behavior for the composite from 0 to 500 V (Fig. 5.5). For the highest gold particle loading (~30% wt/wt PmPV), the conductivity increases from 3.5×10^{-9} S/m for pure PmPV to 9×10^{-8} S/m for the Au/PmPV nanocomposite (30% wt/wt).

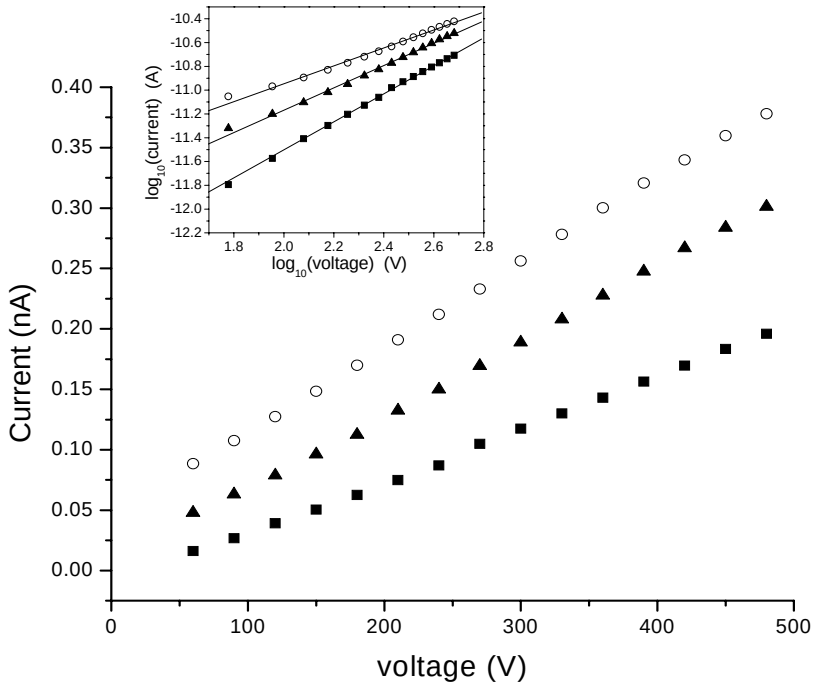

Fig 5.5 A plot of current vs voltage for pure PmPV (■), 15% wt/wt concentration of gold particles in PmPV (▲) and 30% wt/wt gold particles in PmPV(○). Inset: Corresponding logarithmic current – voltage characteristic.

Standard conductivity in polymers is determined by the conjugation, trap density and π-π* gap, as well as ease of charge transfer from one chain to another. In

fact, if the hopping between polymers is too great we induce a deep trap, which will debilitate the charge transfer process. The presence of the metal particles is used to see if they could enhance the conductivity of the samples. Although we have seen a slight increase in the conductivity by their presence, we did not observe the expected percolation effect normally seen in composite materials when we combine polymers and metallic particles. For a greater concentration of gold particles we would expect there to be a percolation increase in conductivity. However, the purpose of these particles is to enhance the conductivity at low loadings. We can see this is not the case, even though comparable loadings of carbon black and nanotubes have demonstrated this in the past [37]. This result may be due to the passivation process whereby the entrapement of the gold particles in the conjugated polymeric matrix has increased the bandgap and thus the hopping distance between charge carriers.

5.4 Polymer, Single Wall Nanotube, and Dye Composite.

We present the transport study of Eosin_SWNT and Polythiophene 506 composite. We study the electrical transport property of the composite to investigate the effects of Eosin_SWNT on the conductivity of the polymer. Fig. 5.6 shows the conductivity of the composite for different loadings of Eosin_SWNT in polythiophene. The percolation threshold of conductivity is 6.84% and the parameter *b* is approximately 0.41.

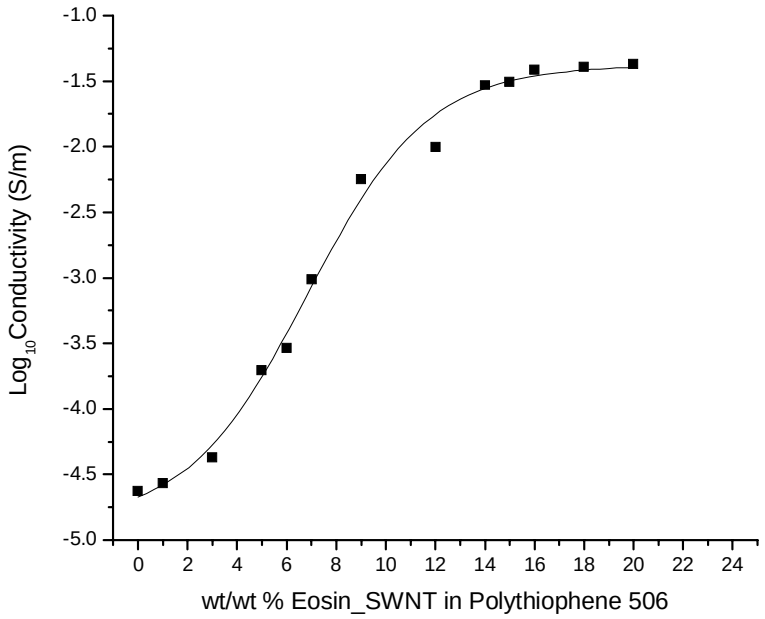

Fig 5.6 Conductivity plot of Eosin_SWNT in Polythiophene 506

The electrical transport study of all the composites such as PmPV-C_{60}, Polystyrene-MWNT, PmPV-Gold, and Eosin-SWNT-Polythiophene composites has shown an increase in conductivity relative to the conductivity of the corresponding pristine materials. By adding either C_{60} or Gold to the PmPV matrix, we have been able to get an increase in conductivity. Polystyrene-MWNT composite has shown a two profile percolation with very low threshold concentrations. By attaching an optically active dye, Eosin, to SWNT-Polythiophene, we have been able to get an increase both in conductivity and absorption. Based on these results, we concluded that these composites are good candidates for device application. We made devices from these composites and characterized electrically. The results are given in the next chapter

6. SCHOTTKY DIODES

In this chapter we present the study of the Schottky diodes made from nanocomposites. The devices are made on glass-ITO substrates using aluminium (Al) evaporated on top of the composite and gold (Au) metal contacts, as shown in Fig. 6.1. These devices are tested for Schottky effect. Schottky diodes with near ideal electrical characteristics were realized.

Two parameters frequently used to describe the forward bias *J-V* relation are the diode quality factor *n* and the barrier heights ϕ_b. These parameters can directly be derived from the *J-V* equation of the Scottky diode.

$$J = J_o\,[exp(qV/nkT) - 1] \tag{6.1}$$

Here, *J* is the total current density, J_o is the value of the reverse saturation current density, *q* is the charge of an electron, *V* is the applied voltage, *k* is Boltzmann's constant, *T* is absolute temperature, and *n* is the diode quality (ideality) factor. An explicit relationship between the barrier height ϕ_b and J_o can be obtained from thermionic emission/diffusion theory as:

$$J_o = A^{**}T^2\,[exp(-q\phi_b/kT)] \tag{6.2}$$

where A^{**} is the modified Richardson constant. For an electron in free space, A=120 A/cm^{2}K^2. The slope of the logarithmic plot is related to the quality factor *n* through:

$$\frac{1}{n} = \frac{\mathrm{kT}}{\mathrm{q}}\frac{\partial \ln \mathrm{J}}{\partial \mathrm{V}} \tag{6.3}$$

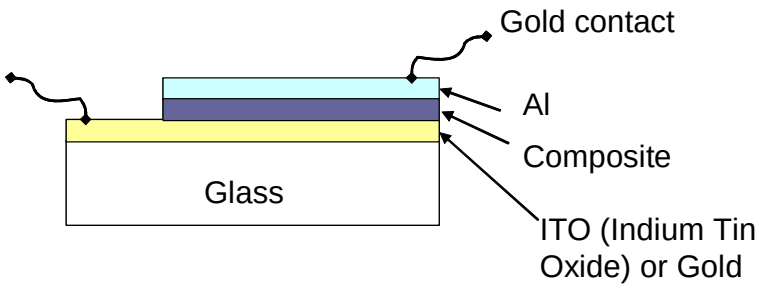

Fig. 6.1 Sandwich cell for device testing

6.1 Polymer-Gold composite

Polymer-Gold composite(1)

In chapter 5 we studied the electrical transport property of PmPV-Au composite. We have seen only a slight increase in conductivity for large loadings of gold in the polymer matrix. However, interesting results are observed in the electrical behavior of sandwich cells made from PmPV-Au composite. The device made out of this composite does behave as a Schottky diode with an ideality factor close to one. Fig. 6.2(a) and 6.2(b) shows the electrical behavior of Al/PmPV/Au and Al/PmPV-Gold/Au sandwich cells, repectively. We have calculated the device parameters from the logarithmic current density versus voltage plots. The sandwich cells behave as a Schottky diode, with different ideality factors and barrier heights. The ideality factors are 10.86 and 1.32 for PmPV and PmPV-gold nanocomposite cells, respectively. The barrier heights, calculated from the reverse saturation current, are 1.24 eV for PmPV and 0.539 eV for PmPV-gold nanocomposite cells.

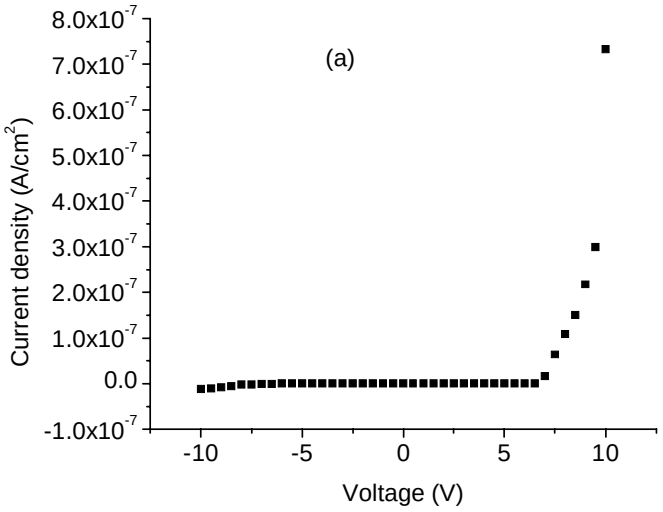

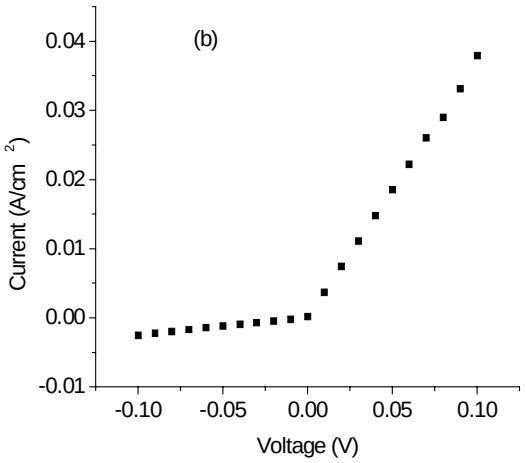

Fig 6.2 J-V plot of (a) Al/PmPV/Au cell; and (b) Al/PmPV-gold nanocomposite/Au cell

Polymer-Gold composite(2)

Fig. 6.3 shows current density versus voltage plot for pure PmPV. The inset is the current density versus voltage plot for PmPV-gold nanocomposite. The plots reveal onset voltages of 1.5V for pure

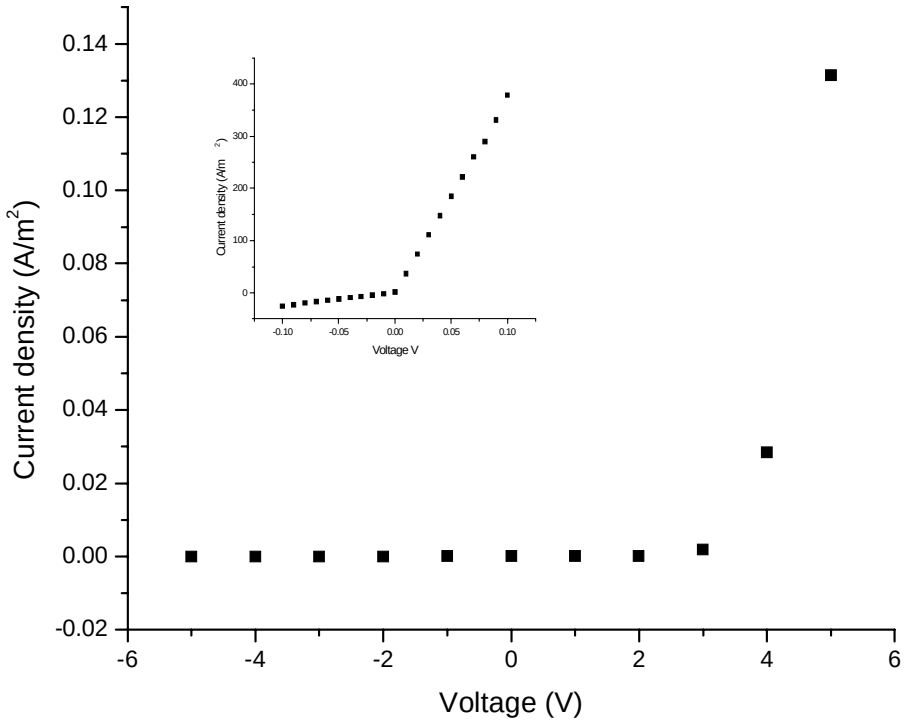

Fig 6.3 J-V plot of Al/PmPV/Gold sandwich cell with inset of Al/PmPV-Au composite/Gold cell.

PmPV and 0.01V for the composite. The sandwich cells behave as Schottky diodes, with different ideality factors n and barrier heights ϕ_b. The values of these parameters have been extracted from the *J-V* plot using (6.2) and (6.3). The ideality factors were calculated to be 27.69 and 1.85 for PmPV and the PmPV-gold nanocomposite cells, respectively. The barrier heights, calculated from the reverse saturation current, are 0.801 eV and 0.616 eV for PmPV and the PmPV-gold

nanocomposite cells, respectively.

From these results, it is deduced that the chemico-incorporation of nano-sized gold particles into the polymer matrix has greatly enhanced the quality of the diode, allowing for better homogeneity of the barrier height over the interface (as compared to the pure PmPV cell). The presence of the nanoparticles enhances band bending at the polymer/Al interface. In addition, at higher ideality values, the recombination current is believed to dominate the diffusion current. The low ideality values for these nanocomposite diodes suggest that the current flow is diffusion or surface/interface dominated. Metallic nanoparticles near the interface may lower the barrier height or the depletion layer, thereby enhancing the charge transport across the interface [55],[222],[265].

6.2 Polymer, Single Wall Nanotube, and Dye Composite.

We study the electrical transport property of a device made from a pure polymer and a composite. We make devices of the composite with concentrations 0%, 6%, and 7% Eosin_SWNT in polythiophene 506 and I-V measurement of the devices are taken with Keithley 6487 Picoammeter/voltage supply instrument.

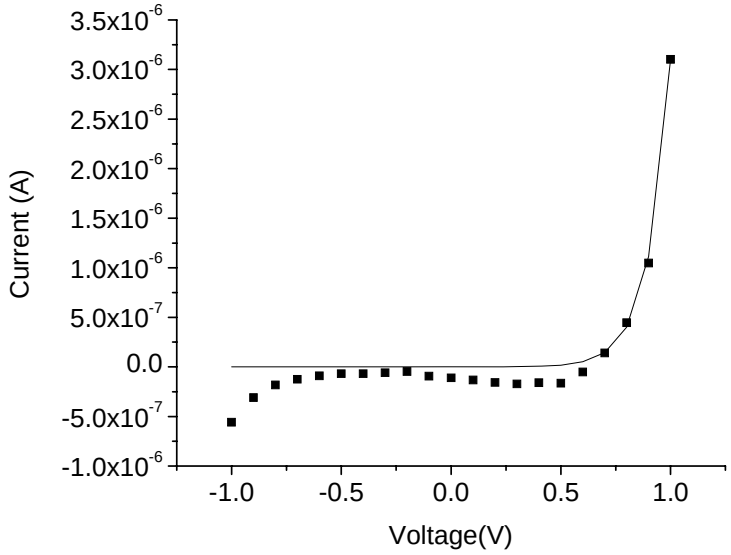

a)

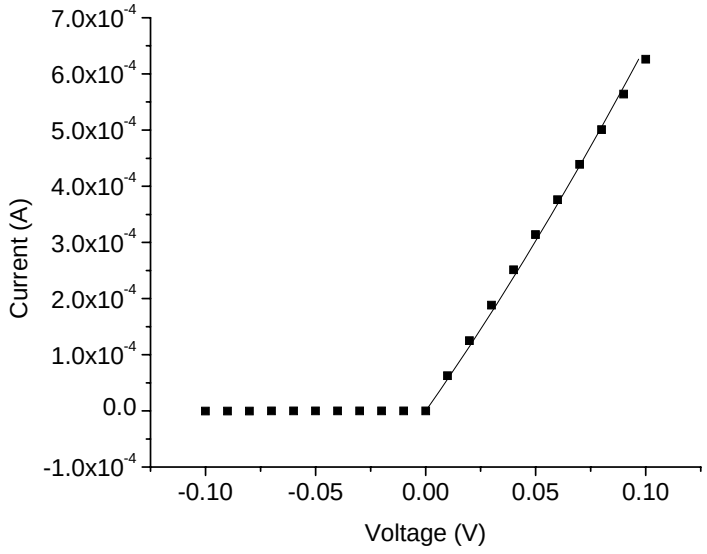

(b)

Fig 6.4 The current voltage plots of the device made of pure polymer (a) and 6% eosin-SWNT in polythiophene (b). The dots represent experimental values while the solid line is a curve fit.

Fig. 6.4 shows the plots for both the polymer (a) and the 6% concentration solution composite (b). The results of the 6% and 7% (not presented here) concentrations are identical. Both the pure polymer and the composite show Schottky effect with different quality factor *n* and barrier potential ϕ_b. The calculated values of *n* are 3.912 and 2.45 for the polymer and the composite, respectively. The barrier height of the device made from the polymer is 1.135 eV and that of the composite device is 0.703 eV. The parameters of the pure PmPV device are found from equation (6.1) where as that of the composite device are found from equation (6.4). This equation involves a series resistance R_s. The valve of R_s is found from the fitting curve and it is 90Ω.

$$I = I_0 \left[EXP\left(\frac{q(V - IR_s}{nkT} \right) - 1 \right] \tag{2.4}$$

From the values of the ideality factor and the barrier height, we can conclude that we make a device with better performance. Forming the composite enables us to get a smooth and lower barrier height. The uniformity of the barrier height over the junction increases the quality of the device

7. CONCLUSION

7.1 Summary

In the previous chapters, we have provided a thotough literature review and provided the experimental work of this study. The literature review included the theoretical background of charge transport and review of research advances and challenges in the application of organic semiconductors in optoelectronic devices such as solar cells, OLEDs, and FETs. The experimental part included electrical transport, spectroscopy, and device fabrication and analysis.

In Chapter 2, it has been discussed that the charge transport in organic semiconductors occurs by the hopping of charges between localized states. Different models have been presented to account for the charge localization effect and verify the experimental results. Those models are: Hopping in a Disordered Medium, The Polaron Model, and Hopping in a disordered medium including polarons. The models correctly predict the temperature and field activation dependence of mobility in disordered organic materials. But they differ as to the functional dependencies. It was demonstrated that the interplay between the polaronic and disorder effects may be responsible for the specific temperature dependence. The basic theoretical and semi-empirical physical concepts used to describe the transport properties of conjugated polymer-metal interfaces have also been presented. In the charge transport across Metal-Semiconductor junction, different charge transport mechanisms exist. These are: Thermionic emission, Generation recombination, quantum mechanical tunneling,

and leakage currents. The thermionic emission equation is used to extract important parameters of the Schottky device.

The review of the three different device applications of organic semiconductors and metal semiconductor junction has also been presented in Chapter 3. The devices are solar cells, light emitting diodes, and field effect transistors. Evidence of the considerable progress that has been made in the field and some commercial products on the market have been mentioned. The main challenges remaining for those devices are low mobility, degradation of the device under operation, and high contact resistance.

The experimental work of this study is presented in chapters 4, 5, and 6. In chapter 4, we presented the spectroscopic study of various nanomaterials and composites. All the spectroscopic results (absorption, fluorescence and Raman spectroscopies) of PmPV-C_{60} confirmed the existence of an electron transfer from the conjugated polymer PmPV to C_{60}. By attaching an Eosin dye to single wall carbon nanotube, we have been able to increase the range of optical absorption of the polymer, nanotube, and dye composite. In chapter 5 conductivity studies of different composites have been presented. A significant increase in conductivity has been achieved by composites made from polystyrene and multi-wall carbon nanotubes. The conductivity plot of the composite shows two distinct transport regions associated with nanotube loadings and corresponding polymerization. These regions suggest two different charge transport mechanisms: charge hopping in low MWCNT loadings (0.02-0.6 wt %) and ballistic quantum conduction in high loadings (0.6-0.9

wt %).

Schottky devices made from Polymer-Gold and P3HT-SWNT_Eosine composites have been presented in chapter 6. The devices made from the composites have a better ideality factor than those that are made of pristine polymers. The ideality factors are 10.86 and 1.32 for PmPV and PmPV-gold nanocomposite cells, respectively. The device made from P3HT-SWNT_Eosine composite has an ideality factor of 1.309. In general all the devices made from the composites have shown a decrease in barrier height.

7.2 Suggestions for further research

In this work, we have been able to make composites with good optoelectronic properties. We made devices from composites and the devices show good performance. Therefore studying those composites for solar cell, OLED, and OFET applications would be a natural extension of this work.

Electrical transport study of polymer-gold composite has shown an increase in conductivity as the gold concentration increases. The device made from the composite has also shown a better diode quality factor than that of the device made from pristine polymer. This research shows that this polymer-gold composite can be a good candidate for OLED applications, since OLEDs operate on the basis of the Schottky effect.

The composite made from polymer, single wall nanotubes, and dye has shown an increase in conductivity as the concentration of nanotubes increases. The device

made from this composite has a better ideality factor than that of the device made from pure polymer. This composite has also shown an increased absorption range in the solar spectrum. This has happened because of the fact that the attached dye is an optically active material. All those results indicate that this composite is a good candidate for solar cell application. For a composite material to be applicable for solar cells, it should satisfy the requirements of good conductivity and absorption.

The research on polystyrene-MWNT and C_{60}-PmPV composites has been done only in terms of spectroscopy and conductivity. The studies show very interesting results. An interesting topic would be, for example, further examination of the composites for device applications. Specifically, the polystyrene-MWNT composite has shown two profile percolation conductivities. These very large increases in conductivity are critical for applications in both solar cells and OLEDs.

REFERENCES:

[1] Adachi, C; Baldo, M. A.; & Forrest, S. R., "Electroluminescence mechanisms in organic light emitting devices employing a europium chelate doped in a wide energy gapbipolar conducting host, "*J. Appl. Phys.* 87 (2000) 8049

[2] Adam, P.; Royer, P.; Laddada, R.; & Bijeon, "Apertureless Near-Field Optical Microscopy: Influence of the Illumination Conditions on the Image Contrast," J., *Applied Optics,* 37 (1998) 1814-1819

[3] Antonietta Loi, M.; Denk, P.; Hoppe, H.; Neugebauer, H.; Winder, C.; Meissner, D.; Brabec, C.; Sariciftci, N. S.; Gouloumis, A.; Vazquez , P.; & Torres,T. "Long-lived photoinduced charge separation for solar cell applications in phthalocyanine–fulleropyrrolidine dyad thin films," *J. Mater. Chem*, 13 (2003) 700-704

[4] Arbogast, J. W.; Darmanyan, A. P.; Foote, C. S.; Rubin,Y.; Diederich, F. N.; Alvarez, M. M.; Anz, S. J.; Whetten, R. L. "Photophysical properties of $C_{60,}$" *J. Phys. Chem*. 95 (1991) 11-12

[5] Arici, E.; Hoppe, H.; Schäffler, F.; Meissner, D.;Malik, M. A.; & Sariciftci, N. S. " Morphology effects in nanocrystalline $CuInSe_2$-conjugated polymer hybrid systems," *Appl. Phys. A* 79 (2004) 59-64.

[6] Arici, E.; Sariciftci, N. S.; & Meissner, D. "Hybrid solar cells based on nanoparticles of $CuInS_2$ in organic matrices," *Adv. Funct. Mater.* 13 (2003) 165.

[7] Arkhipov, V. I.; Heremans, P.; Emelianova, E.V.; Adriaenssens, G.J.; Bässler, H., "Equilibrium trap-controlled and hopping transport of polarons in disordered materials," *Chemical Physics* 288 (2003) 51

[8] Arkhipova, V. I.; Heremans, P.; Emelianova, E. V.; Adriaenssens, G. J.; & Bässler, H., "Charge carrier mobility in doped semiconducting polymers," *Applied Physics Letters*, 82 (2003) 3245

[9] Bao, Z.; Lovinger, A. J.; Brown, J. "New Air-Stable *n*-Channel Organic Thin Film Transistors," *J. Am. Chem. Soc*. 120 (1998) 207-208.

[10] Bartic, C.; Campitelli, A.; Borghs, S. "Field-effect detection of chemical species with hybrid organic/inorganic transistors," *Appl. Phys. Lett*. 82 (2003) 475-477.

[11] Bässler, H.; “Charge Transport in Disordered Organic Photoconductors a Monte Carlo Simulation Study,” *Phys. Status Solidi* B 175(1993) 15-56.

[12] Bässler, H.; Borsenberger, P.M.; Perry, R. “Charge transport in poly(methylphenylsilane): The case for superimposed disorder and polaron effects,” J. *Polym. Phys.* 32 (1994) 1677.

[13] Baude, P. F.; Ender, D. A.; Haase, M. A.; Kelley, T. W.; Muyres, D. V.&Theiss, S. D. “Pentacene-based radio-frequency identification. Circuitry,” *Appl. Phys. Lett. 82* (2003) 3964–3966.

[14] Beek, W. J. E.; Wienk, M. M.; & Janssen,R. A. J. “Efficient hybrid solar cells from ZnO nanoparticles and a conjugated polymer,” *Adv. Mater.* 16 (2004) 1009.

[15] Beek, W. J. E.; Wienk, M. M.; Kemerink, M.; Yang, X..; Janssen, R. A. J “Hybrid zinc oxide conjugated polymer bulk heterojunction solar cells,” *J. Phys. Chem. B* 109 (2005) 9505.

[16] Bergmann, R. B., “Crystalline Si thin-film solar cells: a. review,” *Appl. Phys. A* 69, 187–194 (1999)

[17] Betzig E., Trautman J. K.; Harris T. D.; Weiner J. S.; Kostelak R. L., “Breaking the Diffraction Barrier: Optical Microscopy on a Nanometric Scale,” *Science* 251 (1991) 1468 [259]

[18] Blake, R.; Gun'ko, Y. K.; Coleman, J.; Cadek, M.; Fonseca, A.; Nagy, J. B.; & Blau, W. J. “A generic organometallic approach toward ultra-strong carbon nanotube-polymer composites,” *J. Am. Chem. Soc.* 126, 10226 (2004).

[19] Blom, P. W. M.; de Jong, M. J. M. & Vleggaar,J. J. M. “Electron and hole transport in poly(p-phenylene vinylene) devices,” *Appl. Phys. Lett.* 68 **(**1996) 3308

[20] Borsenberger, P. M.; & Bässler, H. “Concerning the role of dipolar disorder on charge transport in molecularly doped polymers,” *J. Chem. Phys.* 95 (1991) 5327

[21] Borsenberger, P. M.; & Weiss, D. S. *Organic Photoreceptors for Imaging Systems (*Dekker, New York, 1993).

[22] Brabec, C. J.; Dyakonov,V.; Sariciftci, N. S.; Graupner, W.; Leising, G. J.; Hummelen, C. “Investigation of photoexcitations of conjugated polymer/fullerene composites embedded in conventional polymers,” *Journal of Chemical Physics*, 109 (1998) 1185-1195

[23] Brabec C J, Sariciftci, N. S. Hummelen, J. C. “Plastic solar cells,” *Adv. Funct. Mater,* 11 (2001) 15-26

[24] Brabec, C. J.; Cravino, A.; Meissner, D.; Sariciftci, N.S.; Rispens, M.T.; Sanchez, L.; Hummelen, J.C.; Fromberz, T. “The influence of materials work function on the open circuit voltage of the plastic solar cells,” *Thin solid films*, 403 (2002) 368.

[25] Brabec, C. J. “Organic photovoltaics: Technology and market,” *Sol. Energy Mater. Sol. Cells,* 83 (2004) 273-292

[26] Braun, D.; Heeger, A. J. “Visible light emission from semiconducting polymer diodes," *Appl. Phys. Lett.* 58 (1991) 1982-1984.

[27] Breeze, A. J.; Schlesinger, Z.; Carter, S. A.; Ho¨rhold, H.-H.; Tillmann, H. *Sol. Energy Mater. Sol. Cells,* 83 (2004) 263-271.

[28] Brown, A. R.; Jarret, C. P.; de Leeuw, D. M.; Matters, M. “Field-effect transistors made from solution-processed organic semiconductors,“*Synth. Met*. 88 (1997) 37.

[29] Buckley A R, Rahn, M. D.; Hill, J.; Cabanillas-Gonzalez, J.; Fox, A. M.; Bradley, D. D. C. “Energy transfer dynamics in polyfluorene-based polymer blends,” *Chem. Phys. Lett.* 339 (2001) 331-336

[30] Bulovic, V.; Kozlov, V. G.; Khalfin, V. B.; Forrest, S. R. “Transform-Limited, Narrow-Linewidth Lasing Action in Organic Semiconductor Microcavities,” *Science,* 279 (1998) 553.

[31] Burgi, L.; Richards, T. J.; Friend, R. H.; Sirringhaus, H. “Close look at charge carrier injection in polymer field-effect transistors,” *Journal of Applied Physics* 94 (2003) 6129.

[32] Burroughes, J. H.; Bradley, D. C.; Brown, A. R.; Marks, R. N.; ackay, K.; Friend, R. H.; Burns, P. L.; Holmes, A. B. “Light-Emitting Diodes Based on Conjugated Polymers,” *Nature* 347 (1990) 539- 541.

[33] Cao, T.; Wei, F.; Yang,Y.; Huang, L.; Zhao, X.; & Cao, W. "Microtribologic properties of a covalently attached nanostructured self-assembly film fabricated from fullerene carboxylic acid and diazoresin," *Langmuir* 18 (2002) 5186

[34] Choudhury, K. R.; Sahoo, Y.; Ohulchanskyy, T. Y.; Prasad, P. N. *Appl. Phys. Lett.* 87 (2005) 73.

[35] Coakley, K.; Liu, Y; McGehee, M. D.; Frindell, K. L.; Stucky, G. D. *Adv. Funct. Mater.* 13 (2003) 301.

[36] Coakley, K.; McGehee, M. D. "Photovoltaic Cells Made from Conjugated **...** Infiltrated into Mesoporous Titania," *Appl. Phys. Lett.* 83 (2003) 3380.

[37] Coleman, J. N.; Curran, S., Dalton, A.B.; Davey, A.P.; McCarthy, B.; Blau, W.; Barklie, R.C. "Percolation-dominated conductivity in a conjugated-polymer-carbon-nanotube composite," *Phys. Rev.* B, 58 (1998) 7492

[38] Coleman, J. N.; Curran, S; Dalton, A.B.; Davey, A.P.; McCarthy, B.; Blau, B; Barklie, R.C. "Physical doping of a conjugated polymer with carbon nanotubes," *Synthetic Metals* 102 (1999) 1174-1175

[39] Conwell, E. M.; "Impurity band conduction in germanium and silicon", *Phys. Rev*. 103 (1956) 51.

[40] Coratger, R.; Girardin, C.; Beauvillain, J.; Dharmadasa, F. M.; Samanthilake, A. P.; Frost. J. E. F.; Prior, K. A.; Cavenett, B. C "Schottky barrier formation at metal/n-ZnSe interfaces and characterization of Au/n-ZnSe by ballistic electron emission microscopy," *J. Appl. Phys.* 81 (1997) 7870

[41] Cravino, A.; Zerza, G.; Neugebauer, H.; Maggini, M.; Bucella, S.; Menna, E.; Svensson, M.; Andersson, M. R.; Brabec, C. J.; & Sariciftci, N. S. *J. Phys. Chem*. B 106 (2002) 70

[42] Cravino, A.; & Sariciftci, N. S. "Double-cable polymers for fullerene based organic optoelectronic applications," *J. Mater. Chem*. 12 (2002)1931

[43] Credo, G. M.; Winn, D. L.; Buratto, S. K. *Chem. Mater* 13 (2001) 1258

[44] Crone, B. *et al.*"Large-scale complementary integrated circuits based on organic transistors," *Nature,* 403 (2000) 521-523.

[45] Crone, B. K.; Dodabalapur, A.; Sarpeshkar, R.; Gelperin, A.; Katz, H. E.; Bao, Z. “Organic oscillator and adaptive amplifiers for chemical vapor sensing,” *J. Appl. Phys.* 91(2002) 10140-10146.

[46] Crowell C. R.; & Rideout, V. L. "Normalised Thermionic-Field (T-F) Emission in Metal-Semiconductor (Schottky) Barriers," *Solid State Electronics*, 12 (1969) 89

[47] Curran, S. A.; Ajayan, P. M.; Blau,W. J.; Carroll, D. L.; Coleman, J. N.; Dalton, A. B.; Davey, A. P.; Drury, A.; McCarthy, B.; Maier, S.; Strevens, A. “Composite from PPV and Carbon Nanotubes: A novel material for molecular optoelectronics,” *Adv. Mater.* 10 (1998)1091

[48] Curran, S.; Davey, A. P.; Coleman, J.; Dalton, A.; McCarthy, B.; Maier, S.; Drury, A.; Gray, D.; Brennan, M.; Ryder, K.; de la Chapelle, ML.; Journet, C.; Bernier, P.; Byrne, H. J.; Carroll, D.; Ajayan, P. M.; Lefrant, S.; Blau,W. “Evolution and evaluation of the polymer nanotube composite,” *Synthetic Metals*. 103 (1999) 2559

[49] Dalmas, F.; Chazeau, L.; Gauthier, C.; Masenelli-Varlot, K.; Dendievel, R.; Cavaillé, J. Y.; Forró, L. “Multiwalled Carbon Nanotube/Polymer Nanocomposites: Processing and Properties,” *J. Polym. Sci. B: Polym. Phys*. 43, 1186 (2005).

[50] de Heer, W. A.; Chatelain, A.; Ugaarte, D. “A Carbon Nanotube Field-Emission Electron Source,” *Science* 270, 1179 (1995).

[51] de Pablo, P. J.; Martínez, M.; Colchero, T. J.; Gómez-Herrero, J.; Maser, W. K. Benito, A. M.; Muñoz, E.; A. Baró, M. “Mechanical and electrical properties of nano-. sized contacts on single-walled carbon nanotubes,” *Adv. Mater*. 12, 573 (2000).

[52] Deng, X.; Zheng, L.; Yang, C.; Li, Y.; Yu, G.; Cao,Y. “Polymer photovoltaic devices fabricated with blends MEHPPV and organic small molecules,” *J. Phys. Chem*. B. 108 (2004) 3451

[53] De Vos, A. “Detailed balance limit of the efficiency of tandem solar cells,” *J. Phys. D: Appl. Phys*., 13 (1980) 839-846.

[54] Dimitrakopoulos, C. D.; & Malenfant, P. R. L. “Organic Thin-Film transistors for large area electronics,” *Adv. Mater*. 14 (2002) 99.

[55] Doniach, S.; Chin, K.K.; Lindau, I.; Spincer, W.E. "Microscopic metal clusters and Schottky barrier formation," *Phys. Rev. Lett*. 58 (1987) 591

[56] Donoval, D.; Barus; M. & Zdimal, M. "Analysis of I-V Measurements on PtSi-Si Schottky Structures in a Wide Temperature Range," *Solid State Electronics*, 34 (1991) 1365

[57] Drechse, J.; Mannig, B.; Kozlowski, F.; Gebeyehu, D.; Werner, A.; Koch, M.; Leo, K.; Pfeiffer, M. "High efficiency organic solar cells based on single or multiple PIN structures," *Thin Solid Films* 451 (2004) 515-517.

[58] Dunlap, D. H.; & Kenkre, V. M. "Disordered Polaron Transport: A Theoretical Description of the Motion of Photoinjected Charges in Molecularly Doped Polymers", *Chem. Phys.* 178 (1993) 67.

[59] Dunlap, D. H. "Explanation for the $\sqrt{E}$ -dependent mobilities of charge transport in molecularly doped polymers", *Phys. Rev.* B 52 (1995)

[60] Dunlap, D. H.; Parris, P. E. & Kenkre,V. M. "Charge-Dipole Model for the Universal Field Dependence of Mobilities in Molecularly Doped Polymers", *Physical Review Letters*, 77 (1996) 542

[61] Dyreclev, P. PhD Dissertation ISBN 91-7871-581-4, Linkoping University, Sweden, (1995)

[62] Ebbesen, T. W.; & Ajayan, P. M. "Large-scale synthesis of carbon nanotubes," *Nature* 358 (1992) 220.

[63] Ehrenfreund, E.; Vardeny, Z.; Brafman, O. Horovitz, B. "Amplitude and phase modes in *trans*-polyacetylene: Resonant Raman scattering and induced infrared activity," *Phys. Rev.* B 36 (1987) 1535

[64] Emin, D.; Seager, C. H.; & Quinn, R. K. "Small-Polaron Hopping Motion in Some Chalcogenide Glasses," *Phys. Rev. Lett.* 28 (1972) 813

[65] Emin, D." Phonon-assisted transition rates I. Optical-phonon-assisted hopping in solids," *Adv. Phys.* 24 (1975) 305.

[66] Emin, D., "Low-temperature ac conductivity of adiabatic small-polaronic hopping in disordered systems", *Physial Review B*, 46 (1992) 9419

[67] Facchetti, A.; Yoon, M. & Marks, T. J. "New Opportunities for Organic Electronics," *Adv. Mater*., 17 (2005) 1705

[68] Fang, H.; Wang, S.; Xiao, S.; Yang, J.; Li, Y.; Shi, Z.; Li, H.; Liu, H.; Xiao, S.; & Zhu, D. *Chem. Mater.* 15 (2003) 1593

[69] Feldblum, A.; Kaufman, J. H.; Elemad, S.; Heeger, A. J.; Chung,T. C. & MacDiarmid, A. G. Opto-electrochemical spectroscopy of *trans*-$(CH)_r$, *Phys. Rev.* B 26 (1982) 815

[70] Fishchuk, I. I.; Kadashchuk, A. K.; Bässler, H.; Weiss, D. S. "Nondispersive charge-carrier transport in disordered organic materials containing traps", *Physical Review* B 66 (2002) 205208

[71] Fishchuk, I. I.; Kadashchuk, A.; Bässler, H.; Nespurek, S. "Nondispersive polaron transport in disordered organic solids" *Physical Review* B 67 (2003) 224303

[72] Fishchuk, I. I.; Kadashchuk, A.; Bässler, H.; & Nešpůrek, S. "Hopping polaron transport in disordered organic solids", *Phys. Stat. Sol.,*1 (2004) 152

[73] Forrest, R; & Thompson, M. E. *J. Am. Chem. Soc*.128 (2006) 8108

[74] Fourier, J.; Boiteax, G.; Seytre, G.; & Marichy, G. *Synth. Met*. 84, 839 (1997).

[75] Foygel, M.; Morris, R.; Anez, D. D.; French, S.; & Sobolev, V. L. *Phys. Rev. B* 71, 104201 (2005).

[76] Frank, S.; Poncharal, P. Wang, Z. L.; & de Heer, W. A. *Science* 280, 1744 (1998).

[77] Frenkel, J., *Phys. Rev.* 54 (1938)

[78] Friedman, S. H.; DeCamp, D. L.; Sijbesma, R. P.; Srdanov, G.; Wudl, F.; & Kenyon, G. L. *J. Am. Chem. Soc*. 115 (1993) 6506

[79] Friend, R. H.; Gymer, R. W.; Holmes, A. B.; Burroughes, J. H.; Marks, R. N.; Taliani, C.; Bradley, D. D. C.; Dos Santos, D. A.; Bre´das, J. L.; Lo¨gdlund, M.; Salaneck, W. R. *Nature 397 (1999)* 121.

[80] Fujitsuka, M.; Masuhara, A,; Kasai, H.; Oikawa, H.; Nakanishi, H.; Ito, O.; Yamashiro, T.; Aso, Y.; & Otsubo, T.; *J. Phys. Chem*. B 105 (2001) 9930

[81] Gelinck, G. H.; Geuns, T. C. T.; & de Leeuw, D. M. *Appl. Phys. Lett*. 77 (2000) 1487.

[82] Gelinck, G. H.; Huitema, H. E. A.; Vab Veenendaal, E.; Cantatore, E.; Schrijnemakers, L.; Van Der Putten, J. B. P. H.; Geuns, T. C. T.; Beenhakkers, M.; Giesbers, J. B.; Huisman, B. H.; Meijer, E. J.; Benito, E. M.; Touwslager, F. J.; Marsman, A. W.; Van Rens, B. J. E.; De Leeuw, D. M. *Nat. Mater., 3 (*2004)106-110.

[83] Gill, W. D.; J. *Appl. Phys.* 43 (1972) 5033.

[84] Ginger, D. S.& Greenham, N. C. *Phys. Rev.* B 59 (1999)

[85] Gong X, Iyer P K, Moses D, Bazan G C, Heeger A J and Xiao S S *Adv. Funct. Mater.* 13 (2003) 325

[86] Gong. X.; Ostrowski, J. C.; Bazan, G. C.; Moses, D.; Heeger, A .J.; Liu, M. S.; & Jen, A. K. J *Adv. Mater.* 15 (2003) 45

[87] Granstrom, M. Ph.D. Dissertation, ISBN 91-7871-707-8, Linkoping University, Sweden, (1996)

[88] Granstrom, M.; Petritsch, K.; Arias, A. C.; Lux, A.; Andersson, M. R.; Friend, R. H. *Nature*, 395 (1998) 257.

[89] Green Power Magazine www.greenpowermagazine.com

[90] Green, M. A.; Emery, K.; King, D. L.; Hisikawa, Y. & Warta, W. *Prog. Photovolt: Res. Appl*. 14 (2006) 45–51

[91] Greenham, N. C.; Peng, X. G.; & Alivisatos, A. P. *Phys. Rev.* B 54 (1996)

[92] Gregg, B. A.; Hanna, M. C. *J. Appl. Phys. 93 (2003)* 3605.

[93] Gundlach, D. J.; Lin, Y. Y.; Jackson, T. N.; Nelson, S. F.; Schlom, D. G. *IEEE Electron Device Lett*. 18 (1997**)** 87-89.

[94] Hadziioannou, G. & van Hutten, P. F. *Semiconducting Polymers: Chemistry, Physics and Engineering*, (Wiley-VCH, Weinheim, 2000) 365.

[95] Halls, J. J. M.; Walsh, C .A.; Greenham, N. C.; Marseglia, E. A.; Friend, R. H.; Moratti, S. C.; & Holmes, A .B. *Nature* 376 (1995)

[96] Halls, J. J. M.; Arias, A. C.; MacKenzie, J. D.; Wu, W.; Inbasekaran, M.; Woo, E. P.; Friend, R. H. *Adv. Mater.* 12 (2002)

[97] Hamers, R. J. *Nature,* 412 (2001)

[98] Harbeke, G.; Meier, E.; Kobel, W.; Egli, M.; Keiss, H.; Tosatti, E. *Sol. State Comm*. 55 (1985) 419

[99] Hashimoto, T.; Ishizawa, N.; Mizutani, N.; & Kato, M. *J. Mater. Res.* 23 (1988).

[100] Heeger, A. J.; Kivelson, S.; Schrieffer, J. R.; Su, W. P. "Solitons in conducting polymers," *Rev. Mod. Phys.* 60 (1988) 781.

[101] Holstein, T. *Ann. Phys.* 8 (1959).

[102] Hone, J.; Whitney, M.; Piskoti, C.; & Zettl, A. *Phys. Rev. B* 59, R 2514 (1999).

[103] Hone, J.; Llaguno, M. C.; Nemes, N. M.; A. Johnson, T.; Fischer, J. E.; Walters, D. A.; Casavant, M. J.; Schmidt, J.; & Smalley, R. E. *Appl. Phys. Lett.* **77**, 666 (2000).

[104] Horowitz, G. *Adv. Mater*. 10 (1998) 10.

[105] Hughes, M.; Shaffer, M. S. P.; Renouf, A. C.; Singh, C.; Chen, G. Z.; Fray, D. J.; & Windle, A. H. *Adv. Mater*. 14 (2002) 382.

[106] Huitema, H. E. A., *et al.*, *Nature* 414 (2000) 599.

[107] Hung, L. S. & Chen, C. H. *MSE Rep.* R 39 (2002) 143

[108] Huynh, W. U.; Peng, X. G. & Alivisatos, A. P. *Adv. Mater.*11 (1999)

[109] Huynh, W. U.; Dittmer, J. J. & Alivisatos, A. P. *Science* 295 (2002) 2425.

[110] Huynh, W. U.; Dittmer, J. J.; Libby, W. C.; Whiting, G. L.; Alivisatos, A. P. *Adv. Funct. Mater.* 13 (2003) 73.

[111] Iijima, S. *Nature* 354, 56 (1991).

[112] Innocenzi, P.; & Brusatin, G. *Chem Mater*. 13 (2001) 3126

[113] Jang, Y.; Kim, D. H.; Park, Y. D.; Cho, J. H.; Hwang, M. & Cho, K. *Appl. Phys. Lett*. 88 **(**2006) 072101

[114] Jenekhe, S. A.; Yi, S. *Appl. Phys. Lett. 77 (2000)* 2635-2637.

[115] Jiao, H.; Goh, S. H. & Valiyaveettil, S. *Macromolecules* 35 (2002) 1399

[116] Kaiser, W. J. & Bell, L. D. "Direct investigation of subsurface interface electronic structure by ballistic-electron-emission microscopy" *Phys. Rev. Lett.* 60 (1988) 1406

[117] Katz, H. E.; Lovinger, A. J.; Johnson, J.; Kloc, C.; Siegrist, T.; Li, W.; Lin, Y. Y.; Dodabalapur, A. "A soluble and air-stable organic semiconductor with high electron mobility," *Nature,* 404 (2000) 478.

[118] Kazaoui, S.; Minami, N.; & Tanabe, Y.; H. Byrne, J.; Eilmes, A.; Petelenz, P.; *Physical Review* B 58 (1998) 7689

[119] Kazmerski, L. L. *Renewable and Sustainable Energy Reviews*, 1 (1997) 71

[120] Kenkre, V. M.; Andersen, J. D.; Dunlap, D. H.; & Duke, C. B.; "Unified Theory of the Mobilities of Photo-injected Electrons in Naphthalene," *Phys. Rev. Lett.* 62 (1989) 1165.

[121] Kenkre, V. M.; & Dunlap, D. H. "Charge transport in molecular solids: dynamic and static disorder," *Philos. Mag.* B 65 (1992) 831.

[122] Keogh, S. M.; Hedderman, T. G.; Gregan, E.; Farrell, G.; Chambers, G.; & Byrne, H. J. *J. Phys. Chem*. B 108 (2004) 6233

[123] Keogh, S. M.; Hedderman, T. G.; Ruther, M. G.; Lyng, F. M.; Gregan, E.; Farrell, G. F.; Chambers, G.; & Byrne, H. J. *J. Phys. Chem*. B 109 (2005) 5600

[124] Kesti, T. J.; Tkachenko, N. V.; Yamada, V. H.; Imahori, H.; Fukuzumi, S. & Lemmetyinen, H.; *J. Am. Chem. Soc,* 124 (2002) 8067

[125] Kice, J. I.; & Mavell, E. N. *Modern Principles of Organic Chemistry, 2^2 ed., MacMillan Publishing Co*., (1974).

[126] Kozlov,V. G.; Parthasarathy, G.; Burrows, P. E.; Forrest, S. R.; You, Y.; Thompson, M. E.; *Applied Physics Letter*, 72 (1998) 144.

[127] Kroon, J. M.; Wienk, M. M.; Verhees, W. J. H.; & Hummelen, J. C.; *Thin Solid Films*, 223 (2002) 403.

[128] Kroon, J. M.; Bakker, N. J.; Smit, H. J. P.; Liska, P.; Thampi, K. R.; Wang, P.; Zakeeruddin, S. M.; Gra¨tzel, M.; Hinsch, A.; Hore, S.; Wu¨rfel, U.; Sastrawan, R.; Durrant, J. R.; Palomares, E.; Pettersson, H.; Gruszecki, T.; Walter, J.; Skupien, K.; & Tulloch, G. E. *Prog. Photovolt: Res. Appl*. (in press)

[129] Kupper, C. J.; & Whitfield, G.D. eds, *Polarons and Excitons*, Plenum, NY, (1963)

[130] Kwong, C. Y.; Djurišic, A. B.; Chui, P. C.; Cheng, K. W.; Chan, W. K.; *Chem. Phys. Lett. 384 (2004)* 372.

[131] Kymakis, E; & Amaratunga, G. A. J.; "Single-wall carbon nanotube/conjugated polymer photovoltaic devices," *Applied Physics Letters*, 80 (2002)

[132] Laquindanum, J. G.; Katz, H. E.; Dodabalapur, A.; Lovinger, A. J.; "n-Channel Organic Transistor Materials Based on Naphthalene Frameworks," *J. Am. Chem. Soc.* 118 (1996) 11331.

[133] Laquindanum, J. G.; Katz, H. E.; Lovinger, A. J. *J. Am. Chem. Soc*. 120 (1998**)** 664-672.

[134] Lee, J. I.; Klaerner, G. & Miller, R. D. *Chem. Mater.* 11 (1999) 1083

[135] Lee, J. I.; & Subramanian, V. *IEEE*, (2003) 7803

[136] Lee S. B.; Zakhidov, A. A.; Khairullin, I. I.; Sokolov, V. Y.; Khabibullaev, P. K.; Tada, K.; Yoshimoto K. & Yoshino, K. *Synthetic metals,* (1996) 155

[137] Lee, C. H.; G. Yu, D. Moses, K. Pakbaz, C. Zhang, N. S. Sariciftci, A. J. Heeger, and F. Wudl, *Phys. Rev.* B 48 (1993)

[138] Leng, W.; Wang, C. H.; Asato, A. E.; Kelley, A. M.; *J. Phys. Chem.* A 106 (2002) 9479

[139] Lim ,Y. T.; Lee, H. C.; Lee, T. W. & Park, O. O. *Opt. Mater.* 21 (2003) 585

[140] Ling, M. M. & Bao, Z. *Chem. Mater.16 (* 2004) 4824-4840

[141] Lof, R. W.; van Veenedaal, M. A.; Koopmans, B.; Jonkman, H. T.; & Sawatzky, G. A. *Phys. Rev. Letters*, 68 (1992).

[142] Lonergan, M. “Charge transport at conjugated polymer-inorganic semiconductor and conjugated polymer-metal interfaces,” *Annu. Rev. Phys. Chem.* 55 (2004) 257

[143] Lu, Y.; Solitons and Polaronsin in Conducting Polymers, *World Scientific Publishing Co Pte L. T. D.*, (1988)

[144] Ma, C. M.; Huang, Y.; Kuan, H.; & Chiu, Y. *J. Polym. Sci. B: Polym. Phys*. 43, 345(2005).

[145] Ma, W. L.; Yang, C. Y.; Gong, X.; Lee, K.; Heeger, A. *J. Adv. Funct Mater., 15 (2005)* 1617.

[146] Magin, E. H.; Borsenberger, P.M. “Electron transport in N,N-bis(2-phenethyl)-perylene-3,4: 9,10-bis(dicarboximide),” *J. Appl. Phys.* 73 (1993) 787.

[147] Marcus, R. A. “Nonadiabatic processes involving quantum-like and classical-like coordinates with applications to nonadiabatic electron transfers,” *J. Chem. Phys.* 81 (1984).

[148] Marcus, R. A. “Sutin, Electron Transfer in Chemistry and Biology,” *Biochem. Biophys. Acta* 811 (1985) 265

[149] Marquez, F.; Garcia, H.; Palomares, E.; Fernandez, L.; & Corma, A.; *J. Am. Chem. Soc* 122 (2000) 6520

[150] Martin, A. G. *Prog. Photovolt: Res. Appl*, 9 (2001) 123

[151] Martin A. G. 3rd World Conference on Photowlmic Energy Conversion May 11-18.2003 Osaka, Japan

[152] Matters, M.; de Leeuw, D. M.; Herwig, P. T.; & Brown, A. R.; *Synth. Met*. 102 (1999) 1999.

[153] McCarthy, B.; Coleman, J. N.; Czerw, R.; Dalton, A. B.; in het Panhuis, M.; Maiti, A.; Drury, A.; Bernier, P.; Nagy, J. B.; Lahr, B.; Byrne, H. J.; Carroll, D. L.; & Blau, W. J. *J. Phys. Chem*. B 106 (2002) 2210

[154] McDonald, S. A.; Konstantatos, G.; Zhang, S.; Cyr, P. W.; Klem, E. J. D.; Levina, L.; Sargent, E. H. *Nat. Mater. 4 (2005)*.

[155] Meijer, E. J.; Gelinck, G. H.; van Veenendaal, E.; Huisman, B. H.; de Leeuw, D. M.; & Klapwijk, T. *Applied Physics Letters* 82 (2003) 4576.

[156] Meincke, O.; Kaempfer, D.; Weickmann, H.; Friedrich, C.; Vathauer, M.; Warth, H.; *Polymer* 45, 739 (2004). 17

[157] Mele, E. J.; Hicks, J. C.; *Phys. Rev*. B 32 (1985)

[158] Miller, A.; & Abrahams, E. "Impurity Conduction at Low Concentrations," *Phys. Rev.* 120 (1960) 745.

[159] Miller, R. C.; Heikes, R. R.; & Mazelsky, R. *J. Appl. Phys.* 32 (1961).

[160] Millis, A. J.; Littlewood, P. B.; Shraiman, B. I.; "Double Exchange Alone Does Not Explain the Resistivity of $La_{1-x}Sr_xMnO_3$," *Phys. Rev. Lett.* 74 (1995) 5144.

[161] MIT Workshop on Organic Electronics, Boston, MA, June 2003.

[162] Mitzi, D. A.; Chondroudis, K.; Kagan, R.; *IBM J. Res. Dev*. 2001, *45 2001)*.

[163] Möller, S.; Perlov, C.; Jackson, W.; Taussig, C.; & Forrest, S. R.; *Nature,* 426 (2003)166

[164] Mott, N. F.; Can. *J. Phys.* 34 (1956) 1356.

[165] Nath, S.; Pal, H.; Palit, D. K.; Sapre, A. V.; Mittal, J. P. *J. Phys. Chem*. B 102 (1998) 10158

[166] Lewis, N. S. *et al. Science* 315 (2007)

[167] Necliudov, P. V.; Shur, M. S.; Grundlach, D. J.; & Jackson, T. N. *Solid-State Electronics,* 47 (2003) 259.

[168] Nelson, S. F.; Lin, Y. Y.; Gundlach, D. J.; Jackson, T. N. *Appl. Phys. Lett. 72 (*1998) 1854.

[169] Nelson, J. *Current opinion in Solid State and Materials Science* 6 (2002) 87

[170] Newman, C. R.; Frisbie, C. D.; da Silva Filho, D. A.; Bre´das, J.; Ewbank, P. C.; & Mann, K. R. *Chem. Mater. 16 (*2004) 4436-4451

[171] Njuguna, J.; & Pielichowski, K. *Adv. Eng. Mater*. 6, 193 (2004).

[172] Novikov, S. V.; & Vannikov, A. V. *J. Phys. Chem.* 99 (1995) 14574.

[173] Novikov, S. V.; Dunlap, D. H.; Kenkre, V. M.; Parris, P. E.; Vannikov, A. V.; "Essential Role of Correlations in Governing Charge Transport in Disordered Organic Materials," *Physical Review Letters*, 81 (1998) 4472

[174] O'Regan B. & Gra¨tzel M. "A low cost, high-efficiency solar cell based on dye-sensitized colloidal TiO2 films," *Nature* 353 (1991) 737.

[175] O'Brien, D. F.; Giebeler, C.; Fletcher, R. B.; Cadby, A. J.; Palilis, L. C.; Lidzey, D. G.; Lane, P. A.; Bradley, D. D. C. & Blau, W. *Synth. Met.* 116 (2001) 379

[176] Olbrich A.; Vancea, J.; Kreupl, F. & Hoffmann, H.; "The origin of the integral barrier height in inhomogeneous Au/Co/$GaAs_{67}P_{33}$-Schottky contacts: A ballistic electron emission microscopy study," *J. Appl. Phys.* 83 (1998) 358

[177] Padovani, F. A.; Stratton, R. "Field and Thermionic-Field Emission in Schottky Barriers," *Solid State Electronics*, 9 (1966) 695

[178] Palstra, T. T. M.; Ramirez, A. P.; Cheong, S-W.; & Zegarski, B. R.; Schiffer, P.; Schiffer, P.; & Zaanen, J. "Transport mechanisms in doped LaMnO3: Evidence for polaron formation," *Physical Review B*, 56 (1997) 5104

[179] Pantarotto, D.; Bianco, A.; Pellarini, F.; Tossi, A.; Giangaspero, A.; Zelezetsky, I.; Briand, J. & Prato, M.; *J. Am. Chem. Soc* 124 (2002)12543

[180] Parris, P. E.; Kenkre, V. M.; & Dunlap, D. H. "Nature of Charge Carriers in Disordered Molecular Solids: Are Polarons Compatible with Observations?" *Physical Review Letters*, 87 (2001)

[181] Pei Q. & Yang Y. *J. Am. Chem. Soc.* 79 (1996) 934

[182] Pesavento, P. V.; Chesterfield, R. J.; Newman, C. R.; & Frisbie, C. D.; *Journal of Applied Physics* 96 (2004) 7312.

[183] Petritsch, D. K. PhD Thesis, Organic Solar cell architectures, Cambridge and Graz, July 2000.

[184] Peumans, P.; Bulovic, V.; & Forrest, S. R. *Applied Physics Letters* 76 (2000)

[185] Peumans, P.; & Forrest, S. R. *Applied Physics Letters,* 79 (2001) 126

[186] Peumans, P.; Yakimov, A. & Forrest, S. R. *Applied Physics Reviews*, 93 (2002) 3693

[187] Pines, D.; Can. *J. Phys.* 34 (1956) 1367

[188] Pippenger, P.M.; Averitt, R. D.; Papanyan, V. O.; Nordlander, P.; & Halas, N. J. *J. Phys. Chem*. 100 (1996) 2854

[189] Pope, M.; & Swenberg, C. E. *Electronic Processes in Organic Crystals and Polymers*, 2nd ed. (Oxford University Press, Oxford, (1999).

[190] Pötschke, P.; Bhattacharyya, A. R.; & Janke, A. *Euro. Poly. J.* 40, 137 (2003).

[191] Qi, D.; Fischbein, M.; Drndic, M.; Selmic, S. *Appl. Phys. Lett., 86 (2005)*

[192] Ratner, M. *Nature,* 435 (2005) 489

[193] Ravirajan, P.; Haque, S. A.; Durrant, J. R.; Bradley, D. D. C.; Nelson, J. *Adv. Funct. Mater. 15 (2005)* 609.

[194] Reber, C.; Yee, L.; John, M.; Zink, J. I.;. Williams, R. S.; Tong, W. M.; Ohlberg, D. A. A.; Whetten, R. L.; & Diederich, F. *J. Phys. Chem*, 95 (1991) 2127

[195] Rees, I. D.; Robinson, K. L.; Holmes, A. B.; Towns, C. R.; O'Dell, R. *MRS Bull., 27 (2002)* 451.

[196] Reyes-Reyes, M.; Kim, K.; Dewald, J.; Lopez-Sandoval, R.; Avadhanula, A.; Curran, S.; Carroll, D. L.. *Organic Letters*, 7 (2005) 5749

[197] Rhoderick, E. H., "Metal-Semiconductor Contacts," *IEEE Proceedings-I Solid-State and Electron Devices*, 129 (1982) 1-14

[198] Rhoderick, E. H.; & Williams, R. H. "Metal-Semiconductor Contacts," (Clarendon Press, Oxford), 2nd Edition, 1988

[199] Rogers, J. A., Bao, Z.; Baldwin, K.; Dodabalapur, A.; Crone, B.; Raju, V. R.; Kuck, V.; Katz, H.; Amundson, K.; Ewing, J. & Drzaic, P. *Proc. Natl. Acad. Sci.* 98 (2001) 4835–4840.

[200] Roman, L. S.; Arias, A. C.; Theander, M.; Andersson, M. R.; & Inganas, O. *Brazilian Journal of Physics*, 33 (2003).

[201] Rostalski, J; & Meissner, D. "*Solar Energy Materials and Solar Cells"*, 63 (2000) 37.

[202] Salleo, A.; & Street, R. A. *J. Appl. Phys*. 94 (2003) 471.

[203] Sariciftci, N. S.; Braun, D.; & Zhang, C.; Srdanov, V. I.; Heeger, A. J.; Stucky, G. & Wudl, F. *Applied Physics Letters*, 62 (1993) 585

[204] Sariciftci, N. S.; Kraabel, B.; Lee, C. H.; Pakbaz, K.; & Heeger, A. J.; Sandman, D. J. *Phys. Rev*. B 50 (1994)

[205] Schein, L. B.; Duke, C. B. & McGhie, A. R. *Phys. Rev. Lett.* 40 (1978) 197.

[206] Schein, L. B.; Glatz, D.; & Scott, J. C. "Observation of the transition from adiabatic to nonadiabatic small polaron hopping in a molecularly doped polymer," *Phys. Rev. Lett.* 65 (1990) 472

[207] Schilinsky, P.; Waldauf, C.; & Brabec, C.J. *Appl. Phys. Lett*. 81 (2002).

[208] Schon, J. H.; Kloc, C.; Laudise, R. A.; & Batlogg, B. "Electrical properties of single crystals of rigid rodlike conjugated molecules," *Phys. Rev. B* 58 (1998) 12952.

[209] Schoonveld, W. A.; Oosting, J. B.; Vrijmoeth, J.; & Klapwijk, T. M. *Synth. Met*. 101 (1999) 608.

[210] Schreck, J. O.; *Organic Chemistry : concepts and applications*, *C. V. Mosby, Greeley*, (1937).

[211] Schroeder, D. 1994 *Modelling of Interface Carrier Transport for Device Simulation* (Wien: Springer)

[212] Schroeder, R.; Majewski, L. A. & Grell, M. *Adv. Mater*. 16 (2004) 633

[213] Seki, K.; Tachiya, M. "Electric Field Dependence of Charge Mobility in Energetically Disordered Materials: Polaron Aspects," *Phys. Rev.* B 65 (2001) 14305.

[214] Shaheen, S. E.; Brabec, C. J.; Sariciftci, N. S.; Padinger, F.; Fromherz, T.; Hummelen, J C. *Applied Physics Letters,* 78 (2001) 841

[215] Shen, Y. L.; Hosseini, A. R.; Wong, M. H.; Malliaras, G. G.; *Chem. Phys. Chem* 5 (2004) 16.

[216] Sheraw, C. D.; Zhou, L.; Huang, J. R.; Gundlach, D. J.; Jackson, T. N.; Kane, M. G.; Hill, I. G.; Hammond, M. S.; Campi, J.; Greening, B. K.; Franc, J.; West *J. Appl. Phys. Lett.,* 80 (2002) 1088-1090.

[217] Shirakawa, H; Louis, E. J.; Louis, A. L.; MacDiarmid, A. J.; Chiang, C. K.; Heeger, A. J "Synthesis of Electrically Conducting Organic Polymers: Halogen Derivatives of Polyacetylene, $(CH)_x$," *J.C.S. Chem. Comm*., (1977) 578

[218] Shirley, E. L.; & Louie, S. G. *Phys. Rev. Letters*, 71 (1993).

[219] Sirringhaus, H.; Brown, P. J.; Friend, R. H.; Nielen, M. M.; Bechgaard, K.; Langeveld-Voss, B. M. W.; Spiering, A. J. H.; Janssen, R. A. J.; Meijer, E. W.; Herwig, P.; de Leeuw, D. M. *Nature 401 (*1999**)** 685-688.

[220] Sirringhaus, H.; Tessler, N.; Friend, R. H.; *Synthetic Metals* 102 (1999) 857-860

[221] Smilowitz, L.; Sariciftci, N. S.; Wu, R.; Gettinger, C.; Heeger, A. J.; & Wudl, F. *Phys. Rev*. B 47 (1993)

[222] Smit, G. D. J.; Rogge, S.; Klapwijk, T.M. *Appl. Phys. Lett*. 80 (2002) 2568.

[223] Solomons, T. W. G. *Fundamentals of Organic Chemistry*, *John Willey & Sons, New York*, (!990)

[224] Someya, T.; Kawaguchi, H. & Sakurai, T. *IEEE Solid-State Circuits*, (2004) 288–289.

[225] Someya, T.; Sekitani, T.; Iba, S.; Kato, Y.; Kawaguchi, H. & Sakurai, T. *Proc. Natl. Acad. Sci.* 101 (2004) 9966–9970.

[226] Someya, T.; Kato, Y.; Sekitani, T.; Iba, S.; Noguchi, Y.; Murase, Y.; Kawaguchi, H.; & Sakurai, T.; *PNAS*, 102 (2005) 12321

[227] Song, T.; Goh, S. H. & Lee, S. Y. *Macromolecules* 35 (2002) 4133

[228] Soos, Z. G.; Bao, S.; Sin, J. M.; & Hayden, G.W. "Compensation Temperature in Molecularly Doped Polymers," *Chem. Phys. Lett.* 319 (2000) 631.

[229] Steuerman, D. W.; Star, A.; Narizzano, R.; Choi, H.; Ries, R. S.; Nicolini, C. Stoddart, J. F.; & Heath, J. R. *J. Phys. Chem.* B 106 (2002) 3124

[230] Street, R. A.; & Salleo, A. *Applied Physics Letters* 81 (2002) 2887.

[231] Street, R. A.; Salleo, A.; & Chabinyc, M. *Phys. Rev*. B 68 (2003) 085316.

[232] Stubinger, T.; & Brutting, W. "Exciton diffusion and optical interference in organic donor-acceptor photovoltaic cells," *Journal of applied physics*, 90 (2001) 3632

[233] Su, W. P.; Schrieffer, J. R.; Heeger, A. J. "Solitons in Polyacetylene," *Phys. Rev. Lett.* 42, 1698 (1979).

[234] Subramanian, V.; Frechet, J. M. J.; Chang, P. C.; Huang, D. C.; Lee, J. B.; Molesa, S. E.; Murphy, A. R.; Redinger, D. R.; & Volkman, S. K. *Proceedings of the IEEE*, 93 (2005)

[235] Suh, Y. S.; Ko, S. W; Jung, B. J. & Shim, H. K. *Opt. Mater.* 21 (2003) 109

[236] Sun, B.; Marx, E.; Greenham, N. C. *Nano Lett. 3 (2003)*.

[237] Sun, B.; Snaith, H. J.; Dhoot, A. S.; Westenhoff, S.; Greenham, N. C. *J. Appl. Phys. 97 (2005)* 14 941.

[238] Sze, S. M., "Metal-Semiconductor Contacts," in Physics of Semiconductor Devices, (Publishers: J Wiley & Sons, Singapore), 2nd Edition (1981) 250

[239] Takahashi, T.; Suzuki, S.; Morikawa, T.; & Katayama -Yoshida, H.; Hasegawa, S.; Inokuchi, H.; Seki, K.; Kikuchi, K.; Suzuki, S.; Ikemoto, K.; & Achiba, Y. *Phys. Rev. Letters,* 68 (1992).

[240] Takamoto, T.; Ikeda, E.; Agui, T.; Kurita, H.; Tanable, T.; Tanaka, S.; *Proc. of the 26th IEEE Photovoltaic Specialists Conference.* New York IEEE, (1997) 1031

[241] Tanaka, J. & Tanaka, M., Hand book of conducting polymers vol. 2 edited by Skotheim, T. A. Marcel Dekker, New York, (1986)1269.

[242] Tang, C. W. & Van Slyke, S. A. *Appl. Phys. Lett.* 51 (1987) 913

[243] Tang, C. W.; VanSlyke, S. A.; Chen, C. H. *J. Appl. Phys. 65 (1998)* 3610.

[244] Tkachenko, N. V. ; Rantala, L. ; Tauber, A. Y.; Helaja, J. ; Hynninen, P. H. ; & Lemmetyinen, H. *J. Am. Chem. Soc.* 121 (1999) 9378

[245] Tokuyama, H.; Yamago, S.; Nakamura, E.; Shiraki, T.; & Sugiura, Y.; *J. Am. Chem. Soc.* 115 (1993) 7918

[246] Kelley, T. W.; Baude, P. F.; Gerlach, C.; Ender, D. E.; Muyres, D.; Haase, M. A.; Vogel, D. E. & Steven D. *Chem. Mater.* 16 (2004) 4413.

[247] Treacy, M. M. J.; Ebbesen, T. W. & Gibson, J. M. *Nature* 381, 678 (1996).

[248] Universal Display Corporation, http://www.universaldisplay.com/. Accessed March 15, 2004.

[249] van den Heuvel, D. J.; Chan, I. Y.; Groenen, E. J. J.; Matsushita, M.; Schmidt, J. & Meijer, G. *Chemical Physics Letters*, 233 (1995) 284.

[250] van Hal P. A.; Wienk, M. M.; Kroon, J. M.; Verhees, W. J. H.; Slooff, L. H.; van Gennip, W. J. H.; Jonkheijm, P. & Janssen, R. A. J *Adv. Mater.* 15 (2003)

[251] Videlot, C.; Ackermann, J.; Blanchard, P.; Raimundo, J.; Fre´re, P.; Allain, M.; Bettignies, R.; Levillain, E.; Roncali, J. *Adv. Mater*. 15 (2003) 306-310.

[252] Voss, D. *Nature 407 (* 2000) 442-444.

[253] Waldauf, C.; Scharber, M. C.; Schilinsky, P.; Hauch, J. A.; & Brabec, C. J. *Iournal of Applied Physics*, 99 (2006).

[254] Walker, A. B.; Kambili, A & Martin, S J "Electrical transport modelling in organic electroluminescent devices," *J. Phys. Condens. Matter* 14 (2002) 9825-9876

[255] Wang, C. H. *Journal of Chemical Physics*, 112 (2000) 1917

[256] Wang, X. B.; Liu, Y. Q. & Zhu, D. B. *Adv. Mater*. 14, 165 (2002).

[257] Wang, Y., *Nature*, 356 (1992) 585

[258] Watt, A. A. R.; Blake, D.; Warner, J. H.; Thomsen, E. A.; Tavenner, E. L.; Rubinsztein-Dunlop, H.; Meredith, P. *J. Phys. D 38 (* 2006).

[259] Woo, H. S.; Czerw, R.; Webster, S.; & D. Carroll, L.; Ballato, J.; Strevens, A. E.; O'Brien, D.; Blau, W. J. *Applied Physics Letters*, 77 (2000) 1393

[260] Workalemahu, B., PhD Dissertation ISBN 91-7871-803-1, Linkoping University, Sweden, (1996)

[261] Wu, M. W.; & Conwell, E. M. "Transport in a-Sexithiophene Films," *Chem. Phys. Lett.* 266 (1997) 363.

[262] Xie, Z.; Zhao, Y.; & Niu, X., *Semicond. Sci. Technol*. 21 (2006) 1077–1082

[263] Xue, J. G.; Uchida, S.; Rand, B. P.; Forrest, S. R. *Appl. Phys. Lett. 84* (2004) 3013.

[264] Xue, J. G.; Uchida, S.; Rand, B. P.; Forrest, S. R. *Appl. Phys. Lett. 85 (2004)* 5757-5759.

[265] Yakimov, A. I.; Dvurechenskii, A.V.; Nikiforov, A.I.; Chikovskii, S.V. *J. Exp. Theor. Phys.* 75 (2002) 102.

[266] Yang, J.; Li, L. & Wang, C. *Macromolecules* 36 (2003) 6060

[267] Yiliang, W.; Yuning, L; Gardner, S. & Ong, B. S. *J. Am. Chem. Soc.* 127 (2005) 614-618

[268] Yu, G.; Gao, J.; Hummelen, J. C.; Wudl, F.; & Heeger, A J *Science* 270 (1995) 1789

[269] Yu, W. L.; Pei, J.; Huang, W.; & Heeger; A. J. *Adv. Mater.* 12 (2000) 828

[270] Zhu, Z. T.; Mason, J. T.; Dieckmann, R.; Malliaras, G. G.; Appl. *Phys. Lett*. 81 (2002) 4643.

[271] Zilker, S. J.; Detchverry, C.; Cantatore, E.; & de Leeuw, D. M. *Appl. Phys. Lett*. 79 (2001) 1124.